

FLUID INCISION AND MICROCHEMICAL ANALYSIS OF THE HANSONBURG
MISSISSIPPI VALLEY-TYPE ORE DEPOSITS IN CENTRAL NEW MEXICO - PUTNAM

P20

FLUID INCLUSION AND MICROCHEMICAL ANALYSIS
OF THE
HANSONBURG MISSISSIPPI VALLEY - TYPE
ORE DEPOSITS IN CENTRAL NEW MEXICO

by

Borden R. Putnam III

Submitted in Partial Fulfillment
of the Requirements for the Degree of
Master of Science in Geology

New Mexico Institute of Mining and Technology

Socorro, New Mexico

October, 1980

ABSTRACT

The Hansonburg deposits, located on the easternmost margin of the Rio Grande rift, are hosted in Pennsylvanian Aged limestones and occupy karstified solution-ways developed within local allochthonous, reef-facies areas of the host. The ore exhibits a "coontail" layering reflecting the paragenetic sequence of the mineralization. The paragenesis consists of early silicification of the limestone, followed by the early sulfide phases of galena and sphalerite, with minor accompanying barite. Later stages of mineralization are massive fluorite and barite, and a late, terminated-quartz.

This study consisted both of measurement of fluid inclusion homogenization and freezing temperatures, and extraction and analysis of the inclusion fluids. Fluid inclusions in galena, fluorite and quartz samples taken from several locations along the north-south striking exposure of the mineralization were studied.

Homogenization temperatures range from 210-135 C, while the melting temperatures (-6 to -14 C) reflect salinities of 10-18 eq. wt. % NaCl. Early mineralization is characterized by the higher homogenization temperatures, while the later

mineralization exhibits a cooling trend. No differences in salinity are reflected from early to late mineral phases though a slight increase is noted in a southerly direction through the district.

Homogenization temperatures at the same stage in the district-wide paragenesis show increases localized near certain southeast trending structures. These high homogenization temperatures are paired with very depressed first melting temperatures, which may indicate increased amounts of dissolved calcium in the inclusion fluids.

Analysis of inclusion fluids indicate that the mineralizing solutions are predominantly Na-Cl brines. The compositions are similar to those reported from inclusion analysis of the minerals from the Cave-in-Rock deposits of southern Illinois, and to compositions reported from present day formational waters.

Analyses of inclusion waters in galena reflect increased concentrations in the Ca, K and Cl values for the early mineralizing solutions. These early solutions are otherwise not significantly different from the later, somewhat cooler solutions. Calculation of filling temperatures from Na/K ratios reflect

excellent agreement with the measured homogenization values. Salinity calculations (eq.wt.% NaCl) from analytical data reflect similar agreement with the depressed inclusion melting temperatures. These agreements indicate that the analyses are consistent with inclusion observations. Pb, Fe, Cu, and Zn concentrations range from 10 to 2000 ppm., and remain fairly consistent throughout the paragenesis.

Calculations of $\log f_{CO_2}$ based upon measurements of CO_2 in inclusion waters detected in the vacuum line during extraction yield values of 1.59 and 1.64 for 200 and 150 C. Calculated pH for the mineralizing solutions is 4.5 for both early and late solutions. Activity of H_2S of the fluids calculated from galena equilibrium and analysed Pb values in inclusion waters is -7.11 for the 150 C fluids. No Pb values were obtainable for the galena phase (200 C) due to mineral solubility. Graphical representation of equilibrium relations for galena, sphalerite, pyrite, barite and anhydrite based upon analytical data delineated ranges of -43.0 to -40.0 for $\log f_{O_2}$ and -18.5 to -16.0 for $\log f_{S_2}$ (150 C). Equilibrium calculations assuming anhydrite presence yield $\log SO_4^{=}$ of -5.56 and -4.7 for early and late solutions. Further calculations at 150 C based upon the respective $\log SO_4^{=}$ value and equilibrium of H_2S yield a $\log f_{O_2}$ of -42.95, which

agrees well with the range defined in the graphical representation. Similarly, log f_{S_2} calculated using the equilibrium of H_2S and the log f_{O_2} , yields a value of -17.18, also showing good agreement with the graphical results. PATH (Helgeson et al, 1970) computer program calculations applied to the data agree with the above results.

The calculations indicate that the mineralizing solutions relatively increased in f_{O_2} while decreasing in f_{S_2} through the paragenesis. The data predict a shift from H_2S dominant to $SO_4^{=}$ dominant solutions. Early 200 C solutions favor the sulfides PbS , FeS_2 and ZnS , with oxides magnetite and hematite, while later solutions show a shift from the predominantly sulfide field, into the sulfate and carbonate stability fields. Magnetite and pyrite are no longer in equilibrium, while ZnS , PbS , $PbSO_4$, $PbCO_3$ and hematite are stable. These calculations agree with the mineralization and paragenesis observed in the field.

These analytical results suggest that the mineralization was resultant from primarily a drop in temperature and pressure, and was not related to changes in solution chemistry. Comparison of inclusion analyses to present-day formational waters suggest that the solutions responsible for the mineralization were intra-formational type waters. Field observations

paired with paleogeographic interpretations suggest that these solutions, by utilizing faults related to the juvenile Rio Grande rifting, invaded and occupied pre-existing open space (karst) developed within the reef-facies of the limestone host.

The remarkable tectonic, lithologic, and chemical similarities of this deposit with the Cave-in-Rock deposits of Southern Illinois, suggest a similar genetic origin for the two.

TABLE OF CONTENTS

ABSTRACT	ii
TABLE OF CONTENTS	vii
LIST OF FIGURES	ix
LIST OF TABLES.	xi
ACKNOWLEDGMENTS	xii
INTRODUCTION.	1
Previous Work.	3
GEOLOGIC SETTING.	6
Regional Stratigraphy	6
Precambrian	9
Paleozoic Rocks	10
Council Springs Member	13
Igneous Rocks	17
Structure	18
Capitan Lineament	19
Ore Deposits	27
Mineralization	27
Paragenesis	28
EXPERIMENT	40
Sampling Procedure	40
Fluid Inclusion Study	42
Types of Inclusions	42
Microthermometry	43
Scanning Electron Microscopy	56

Microanalytical Determination	60
Cleaning and Extraction Procedures	60
Leaching Procedure	61
Blanks	63
Artificial Inclusions	64
COMPOSITION OF FLUID INCLUSIONS	67
Thermodynamic Calculations	77
PATH Computer Calculations	95
Chemical Model	97
Depth of Mineralization	97
SOURCE OF MINERALIZING SOLUTIONS	99
GENETIC MODEL	107
DISCUSSION OF SIMILARITIES BETWEEN THE HANSONBURG DEPOSITS AND THE CAVE-IN-ROCK DEPOSITS OF SOUTHERN ILLINOIS	110
Stratigraphy	110
Continental Rifts	110
Lineaments	111
Local Structure	112
Ore Horizon	117
Mineralogy	118
Fluid Inclusions	118
SUMMARY AND CONCLUSIONS	119
REFERENCES	121
APPENDIXES	
A. Tables of Thermodynamic and Experimental Data	A 1-6
B. Fluid Inclusion Study - Observations	B 1-6
C. Fluid Inclusion Study - Procedures	C 1-14

LIST OF FIGURES

Figure	Page
1 General geologic map of the Hansonburg area	8
2 Stratigraphic column for the rock units in the Hansonburg district	12
3 Unmineralized Council Springs Member.	16
4 Regional structure of the Hansonburg area	21
5 Hansonburg district with major structures, and sample sites.	23
6 Mineralized fissure in the Abo Formation	30
7 Mineralized host correlation I	32
8 Mineralized host correlation II	34
9 Generalized paragenetic sequence.	39
10 Fluid inclusion photomicrographs	46
11 Fluid inclusion microthermometry results	48
12 Fluid inclusion microthermometry results plotted against sample location	50
13 Cross-section, sample HSMQ1, with microthermometry data	55
14 Scanning electron photomicrographs	59
15 Calculated Na/K temperatures	75
16 Graphical determination of fO_2 , fS_2	85
17 fO_2 - fS_2 diagram at 200 C	90
18 fO_2 - fS_2 diagram at 150 C	91
19 fO_2 - pH diagrams for 150 and 200 C	94

Figure	Page
20 . Occurrences of galena, barite and fluorite deposits relative to the margins of the Rio Grande rift in New Mexico106
21 General geologic and structural map for the Cave-in-Rock district, southern Illinois116

LIST OF TABLES

Table		Page
I	Analysis of blanks and artificial inclusions	66
II	Fluid inclusion compositions - solution components	71
III	Fluid inclusion compositions - volatiles, molality and atomic ratios . .	72
IV	Averaged inclusion compositions, with 90% confidence limits	73
V	Comparison table of Hansonburg inclusion analyses to those from various other Mississippi Valley-type deposits, and present day formational waters	76
VI	Tabulation of activity coefficients used in thermodynamic calculations . . .	79
VII	Summary of results of thermodynamic calculations	88
VIII	Summary of results from PATH computer program calculations	96

ACKNOWLEDGMENTS

This study was initiated at the suggestion of my advisor Dr. David I. Norman, who is here gratefully acknowledged for his continued advice, guidance and attention throughout the course of the study. Dr. C. J. Popp, and Dr. K.C. Condie, committee members, are thanked for their advice and meticulous review of the manuscript. Dr. Popp also donated the use of the analytical equipment used in this study.

This study would not have been undertaken were it not for the generosity of Dr. Rene' S. Steensma. Dr. Steensma's continued financial support, and loan of field vehicle allowed for a complete examination of the Hansonburg district. The Steensma family is here also thanked for their continued moral support and welcomed suppers.

Dr. F.E. Kottowski, Director; Dr. R.H. Weber and Mr. S. Thompson III of the New Mexico Bureau of Mines and Mineral Resources are thanked for their discussions on various parts of the research. Dr. C.E. Chapin, also of the bureau, is thanked for his personal review, and long discussions over certain aspects of the thesis; Mrs. Lynn Brandvold, chemist, for allowing the use of her laboratory; and the bureau drafting department for their suggestions and painstaking work on the numerous diagrams which accompany this thesis.

Robert W. Smith is thanked for he contributed much time overseeing the numerous thermodynamic calculations. He also performed the computer calculations using a modified version of the PATH program. Mr. John Shortess, photographer for the R.D.D., and Mrs. Karen Emch, who operated the SEM, are both thanked for their excellent work. The entire Geoscience faculty is here acknowledged, for they were each contacted in this study at a point when their expertise was needed. Their suggestions and advice expanded the knowledge peripheral to this study.

Thanks are given to Mr. and Mrs. Sam Jones of Bingham, N.M., who donated time, advice and friendship during the course of the field work. Mr. Sam Jones is especially acknowledged for the accounts of his personal experience in the district.

The author wishes to thank many who were not involved in this study, but without who, the work surely would have suffered: To my wife Ann, for her companionship; to my parents for both their moral and financial support; to the Vigilante Band for their continual distractions; and to Bobby Weir, for his continued inspirations.

INTRODUCTION

The problem of coherent genetic models for Mississippi Valley-type deposits has long been an enigma. A wide variety of models are hotly debated (Brown, 1967), from diagenetic (Davis, 1977) to hydrothermal and a variety of solution mixing models (Ohle, 1980). The pioneering work by White (1958), Beales and Jackson (1966), Ohle (1959) and others suggest the active involvement of basinal, connate water brines in the transport of metals. Doe and Delevaux (1972), on the basis of their lead isotopic study, supported these theories and postulated that the arkosic sediments underlying the ore-zone were the source of the metals.

The data upon which these hypotheses are based have been rapidly growing and are constantly being refined. The use of fluid inclusion analyses together with stable isotope and other geochemical studies have narrowed greatly the acceptable hypotheses. To be applicable, any theory must explain: 1. Location of the districts. 2. Large size of individual districts. 3. Diversity of mineral assemblages and their mode of occurrence. 4. Diversity of host lithology, though carbonate sediments do predominate. 5. The paragenetic sequence, with its local variations or

repetitions of sequence. All these characteristics, along with individual districts unique features, must be addressed in a realistic, comprehensive model.

This study was undertaken to attempt to explain the above characteristics, as observed for the Mississippi Valley-type mineralization developed at Bingham, New Mexico. The study is based on detailed fluid inclusion analyses and consists of: 1. Microthermometry and 2. Microanalysis of the inclusions at distinct points through the mineralization as depicted by the paragenetic sequence. 3. Thermodynamic calculations of the pH, fO_2 and fS_2 of the mineralizing solutions based upon these analyses enabled the determination of thermochemical variations in the fluids extracted from each mineral phase. Various methods of calculation were employed, both by hand and by computer using a modified version of the PATH (Helgeson et al., 1970) program used at New Mexico Institute of Mining and Technology.

A coherent genetic model which satisfies the previously mentioned characteristics is postulated based upon fluid inclusion data, field observations, tectonic setting and paleogeographic interpretations.

The Bingham site was selected because it has been classified as a Mississippi Valley-type deposit (Roedder et al., 1968), and has a mineralogy and

geologic setting similar to the Cave-in-Rock deposits of Southern Illinois (Hall and Friedman, 1963). The Cave-in-Rock deposits are the only Mississippi Valley-type deposits in which the chemistry of the ore-depositing fluids has been studied in detail by inclusion microanalysis. The minerals at Bingham have large primary inclusions which make them particularly suited for this type of work.

Previous Work

The deposit has been well studied. First was the brief mention by Lindgren et al., (1910). Lasky (1932), and Kottowski (1953) published the first detailed reports on the district, and noted its similarity to the Mississippi Valley deposits of the central United States. Kopicki, (1965) and Lewchalermvong, (1973) discussed the general geology and genesis of the deposits.

Slawson and Austin (1960, 1961) and Austin and Slawson (1962) published lead isotope studies on galena samples from a number of central New Mexico deposits, including the Hansonburg. Their results indicate that the Hansonburg district has highly radiogenic or "J" type leads. Beane (1974) interpreted the lead data of Slawson and Austin to indicate the source of the lead

as both the Permian arkosic units (derived from Precambrian granitic rocks), and the Precambrian basement rocks. He indicated intraformational brines heated by shallow mid-Tertiary intrusives for the transport of the ore components. Ewing (1979), reinterpreted Slawson and Austin's results, and presented a model which incorporated leaching of both sediments and basement rocks (after Beane, 1974). Ewing implicates mid to late Tertiary continental rifting and magmatic activity in the development of "widespread but small-scale geothermal systems" and the subsequent formation of "Hansonburg-type deposits".

Roedder et al. (1968) conducted a detailed fluid inclusion study of the Hansonburg deposits, and delineated a paragenetic sequence based in part upon the apparent sequence of fluorite deposition. Their results indicate filling temperatures in the range 200-100 C, and show a slight increase in salinity for later, cooler (100 C) mineralizing fluids.

Allmandinger (1975) conducted an in-depth geochemical study of the deposits, utilizing fluid inclusion and stable isotope data. His results indicate filling temperatures in accord with Roedder et al. (1968), and isotopic data which support a Permian aged source-bed for the origin of the mineralizing solutions.

According to Allmandinger's (1975) model, convection of

these discharged meteoric waters heated by a high regional geothermal gradient, mixed with cooler, more oxygenated solutions, interacted with the host rock, and precipitated the mineralization.

GEOLOGIC SETTING

The geology in the vicinity of the Hansonburg deposit has been described in detail by Wilpolt and Wanek (1951), Kottowski (1953), Kopicki (1963) and Lewchalermvong (1973). Allmandinger (1975) presented a concise description of the area based upon these previous works.

The Bingham mining district is located in the Oscura Mountains which comprise the easternmost margin of the Rio Grande Rift (Fig. 1). The area is characterized by north-south en echelon normal faulting resultant from the rift-related extension which started 32-37 m.y. ago (Chapin, 1979).

Regional Stratigraphy

The basement rocks in the region are granitic crystalline rocks of Precambrian-age. These rocks are unconformably overlain by the Pennsylvanian and Permian Formations, which consist of limestones, sandstones, arkoses and evaporites, and continentally-derived red-beds and other sediments (Fig. 2). Eardley (1962) indicates that large areas of New Mexico were uplifted from Cambrian through Mississippian time, with the shore line near the present day 33-34 standard

Figure 1

Generalized geological map of the Hansonburg district, and immediate vicinity (after Wilpolt and Wanek, 1951).



INDEX MAP

KEY

QUATERNARY



Alluvium

TERTIARY



Intrusive rocks

PERMIAN



Permian formation
(undivided)

PENNSYLVANIAN



Madera Limestone



Sandia Formation

PRECAMBRIAN



Crystalline rocks

FAULTS



normal fault; dashed where
approximately located; † indicates
downthrown side

uncertain position

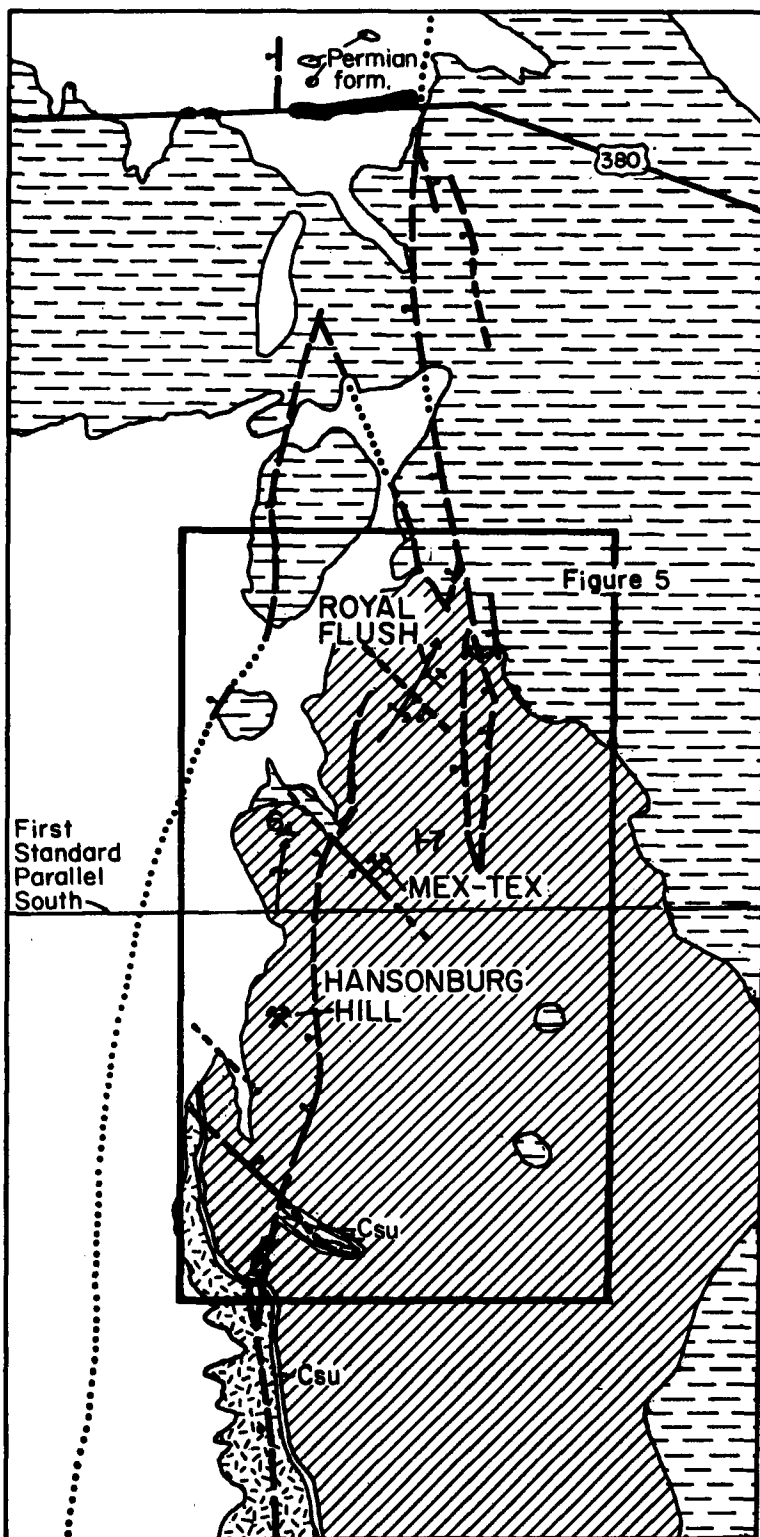
.....
covered fault



anticlinal axes showing
plunge (dashed where
approximately located)



strike and dip of beds



parallel. This would explain both the unconformity observed between the Precambrian basement rocks and the Paleozoic sediments, and the rapid thinning and termination of Cambrian through Pennsylvanian strata as the district is approached from the south. These Paleozoic sediments are intruded by abundant dikes and sills of Cenozoic age (Wilpolt and Wanek, 1951).

Precambrian

The Precambrian-aged rocks are coarse to medium grained, locally pegmatitic granites and gneisses. Large xenoliths of an amphibolite rock are found locally.

Quartz veins from 3-25cm thick randomly cut the Precambrian rocks. The veins carry no sulfides or fluorite, though a few of the veins showed slight iron staining. There was no evidence of vug or open-space filling, with the veins exhibiting only the "bull" type quartz associated with more forceful types of fluid injection. Quartz veins in the Precambrian crystalline rocks do not penetrate the overlying sedimentary section.

The contact between the Precambrian basement and the Paleozoic strata in the vicinity of the Hansonburg is characterized by a thin, darkly colored horizon,

composed of a dark, brittle type of silicified limestone. This contact is void of any observable mineralization.

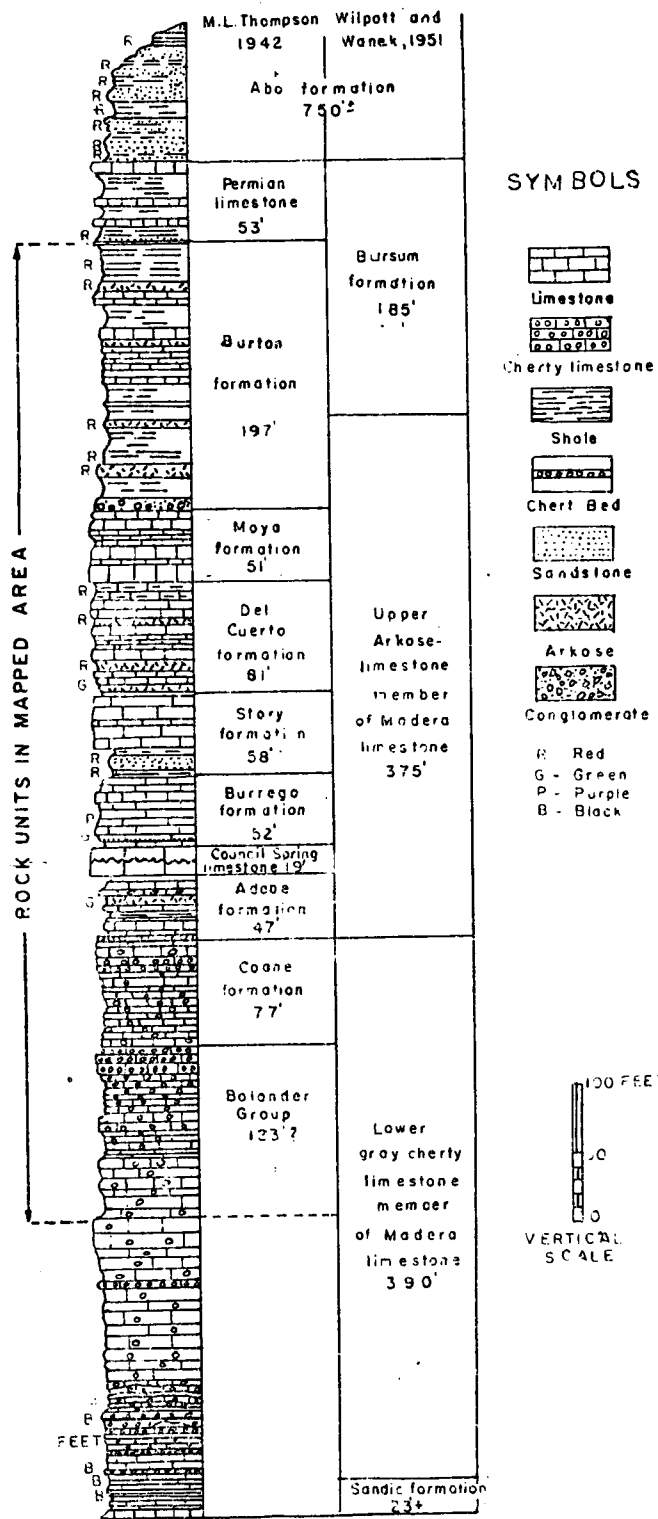
Paleozoic Rocks

Paleozoic rocks in the vicinity of the Hansonburg deposits are limestones, shales and other marine sediments of Pennsylvanian Age (Fig. 2). These units are thin to massively bedded, and contain abundant fossil and organic debris. The Paleozoic section shows remarkable thinning in the area of the Hansonburg. To the south in White Sands Missile Range, the section thickens and becomes more extensive in the basal units. The presence and thickening of these older sediments (Mississippian through Ordovician) to the south, together with the increase in clastic nature of the upper Pennsylvanian strata to the south, suggest the effect of the uplifted Pedernal landmass to the north on sedimentation (Kottlowski, 1960).

Kottlowski (1960) correlated the stratigraphy of southern New Mexico and indicated a paleo-highland in the Hansonburg region throughout Pennsylvanian time (Kottlowski, 1960, plates 2,3). The occurrence of reef facies in the San Andres Mountains suggests biohermallike reefs were numerous relative to their position around the Paleozoic basins (e.g. - Orogrande basin) (Kottlowski, 1960, pl. 3).

Figure 2

Stratigraphic column of the Pennsylvanian and lower Permian rock units in the vicinity of the Hansonburg deposits (after Kottowski, 1953).



After Frank E. Kottlowski

Council Springs Member

The Hansonburg mineralization occurs in the Council Springs Member of the Pennsylvanian Madera limestone (Fig. 2). Minor mineralization is observed only locally in the overlying sedimentary section (Fig. 6).

The Council Springs Member is a silicified, predominantly massive limestone unit which locally grades into a reef facies limestone. This allochthonous limestone unit is characterized by laminated carbonate layers of fine micritic detritus which show slight cross bedding, interbedded with layers of more coarse, fragmental material representing, perhaps, algal or "rip-up" structures (J.D.MacMillan, 1980, oral. commun.). These coarse layers are composed of a variety of fragment sizes, of only slightly varying lithology (Fig. 3A). Silicification of the unit makes identification of these lithic fragments extremely difficult. Most fragments, however, are quite porous and appear to have been originally composed of some carbonate or algal matter. The porous nature of these fragments greatly increase the primary porosity of the limestone unit.

Development of secondary porosity in the unit is best observed in unmineralized sections of the limestone. Here laminated cavities (bedding-plane anastomoses) resultant from dissolution of the coarse fragmental layers are honey-combed with the sinuous fine grained interbeds which reflect original bedding irregularities (Fig. 3B). The alternation of limestone beds of varying purity and differing resistance to dissolution favors the formation of these horizontal cavities during karst activity (Sweeting, 1973). These cavities are the open-space utilized by the later mineralizing fluids.

The presence of preexisting authigenic pyrites is evidenced by the abundant cubic casts and iron oxides. Locally these sulfides appear to have been replaced by galena/barite. Authigenic sulfides are associated with both the coarse rip-up structures and the fine grained interbeds. The presence of sulfides within the limestone suggest a reducing depositional environment. This type of environment is characteristic of an inter-supra tidal zone, which is favorable for the formation of this reef facies-type of limestone. The presence of authigenic sulfides, particularly pyrite, within a limestone greatly enhances the limestone's solubility. Oxidation of the sulfides creates sulfuric acid. Chemical reaction of this acid solution with the

Figure 3

A Allochthonous Council Springs limestone. Note porosity of fragments and their appearance. Large hematite (after pyrite ?) in upper right, and abundant pyrite casts (with iron stains) at lower left. Lower right edge of specimen is margin of larger solution cavity. Note fine detailed solution effects.

B Field photo of more massive sections of the Council Springs showing local bedding-plane anastomoses developed in more porous sections of the unit.

limestone may remain in solution (after the space)
which are typical of the region (see also, 1973,

p21)

the

thou

is a

line

of t

spr

Burk

hist

*pot

Cen

kare

depo

igne

spe

desc

Cen

mine

type

throughout the central part of the region

been related to the regional tectonic



limestone may result in solution caverns (open-space) which are lined with gypsum (CaSO_4) (Sweeting, 1973, p21). Numerous caverns of this type are present within the Hansonburg district, many adjacent to similar, though mineralized, caverns.

The Council Springs Member in the Hansonburg area is unconformably overlain by the more massive limestones of the Burrego Formation and the remainder of the Upper Pennsylvanian section.

The presence of open-space within the Council Springs unit and the disconformable nature of the Burrego-Council Springs contact indicate a depositional hiatus between these two units. The occurrence of "pot-holes" (lapie's ?) at the upper surface of the Council Springs indicates the possibility of karstification of the Council Springs Member prior to deposition of the Burrego Formation (Kopicki, 1963).

Igneous Rocks

Other than the Precambrian rocks previously described, intrusive rocks are considered to be of Cenozoic age. The intrusives occur as dikes, sills and minor stocks of monzonitic, andesitic and dioritic rock types (Wilpolt and Wanek, 1951). Dikes are common throughout the central part of New Mexico, and have been related to both regional extension (Allmandinger,

1975, and others), and the Capitan lineament (Chapin, 1979). The Jones Camp dike, dated at 27.2 ± 1.1 and 29.4 ± 2.0 my. (Allmendinger, 1975), and the numerous other intrusives in the region indicate a mid-Tertiary magmatic episode. Allmendinger suggests that the Jones Camp dike, 6 miles northeast of Hansonburg, is intruded along a structure related to some north-south extension (Fig. 4). Chapin (1979, and others) indicate the alignment of similarly aged intrusives across southern New Mexico, and relate the orientation of these and the Jones Camp dike to the Capitan lineament.

The Hansonburg district contains a smaller dike of similar composition to the Jones Camp dike, which intrudes through the Paleozoic cover on the north end of the Hansonburg Hill. This dike, from 2-4 meters wide, crosscuts the mineralized horizon, and obliterates the mineralization. No sulfides are associated with the dike. Extensive gossan is developed within the carbonates in the immediate vicinity of the dike, resultant from oxidation of the preexisting sulfides of the Hansonburg deposit.

Structure

The Sierra Oscura are characterized by a steep fault scarp on the west and a sloping highland to the east. Displacement along the Sierra Oscura fault is

resultant from Rio Grande Rift extension, of mid-Tertiary age (Chapin, 1979). The throw along the fault increases toward the south from the Hansonburg district, though northward the fault disappears into the Oscura anticline (Fig. 4). Paleozoic strata form the crest of the Oscura range, and outcrop as a series of cuerdas on the sloping highlands to the east (Wilpolt and Wanek, 1951).

The Hansonburg district contains numerous small-scale isolated fault blocks which generally dip eastward at 7° (Fig. 5). Locally strata show drag resultant from the Oscura fault displacement.

Capitan Lineament

A regional structure known as the Capitan lineament (Kelley and Thompson, 1964; Chapin and others, 1978) passes through the Hansonburg region. It trends west-northwest, and is defined in part by the alignment of Tertiary aged intrusives. The alignment of the Jones Camp dike, the basaltic craters of the Carrizozo Malpais, the Capitan intrusive and the lengthy dikes east of Roswell (the Camino del Diablo, Railroad Mtn. and other dikes) suggest a regional control on the intrusion and location of magma bodies by a zone of crustal weakness (Chapin, 1979). In

Figure 4

Regional structure of the Hansonburg area,
and East (after Kelley and Thompson, 1964).
Shaded band marks location of the Capitan
lineament (after Chapin et al., 1978).

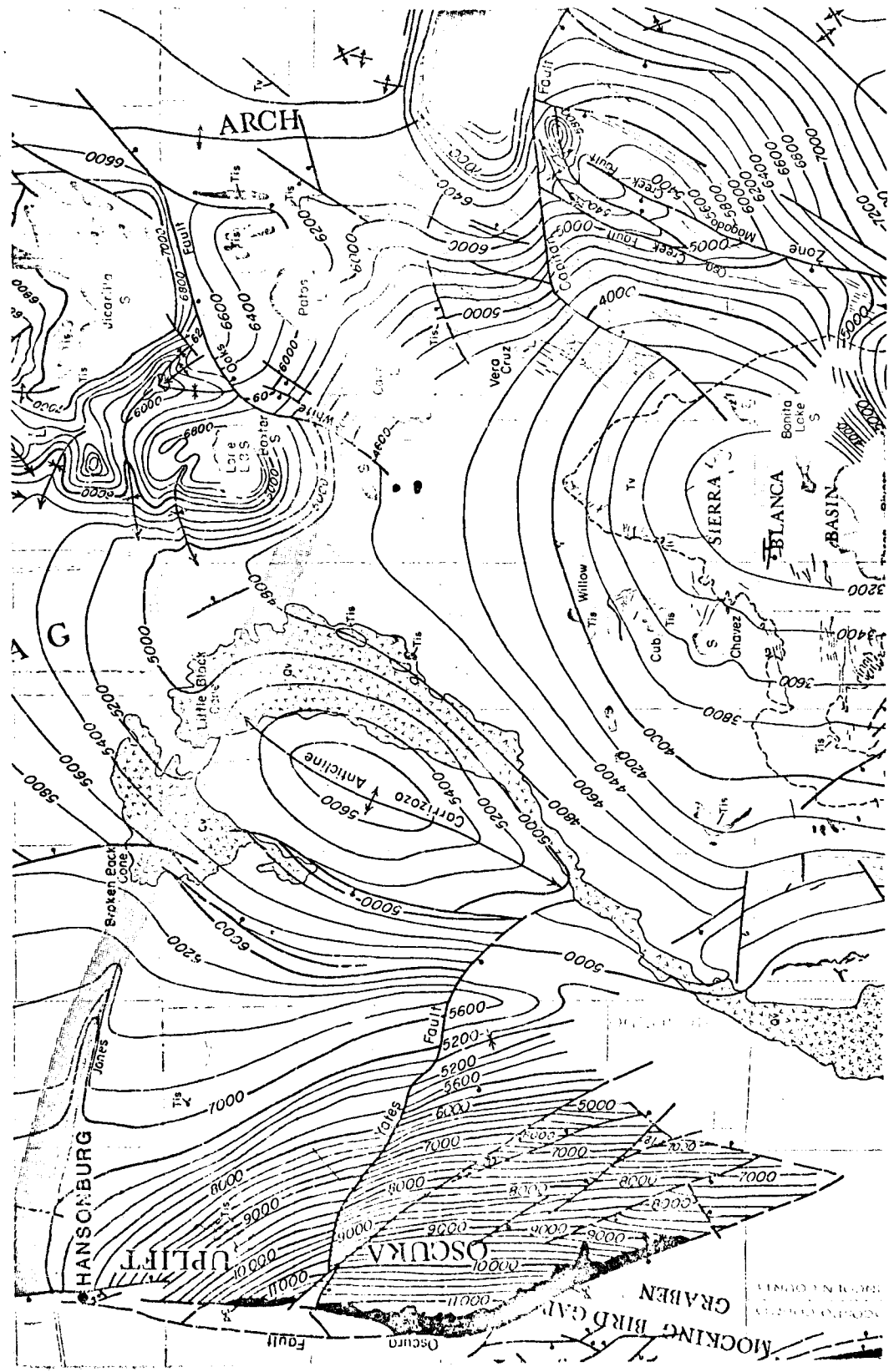
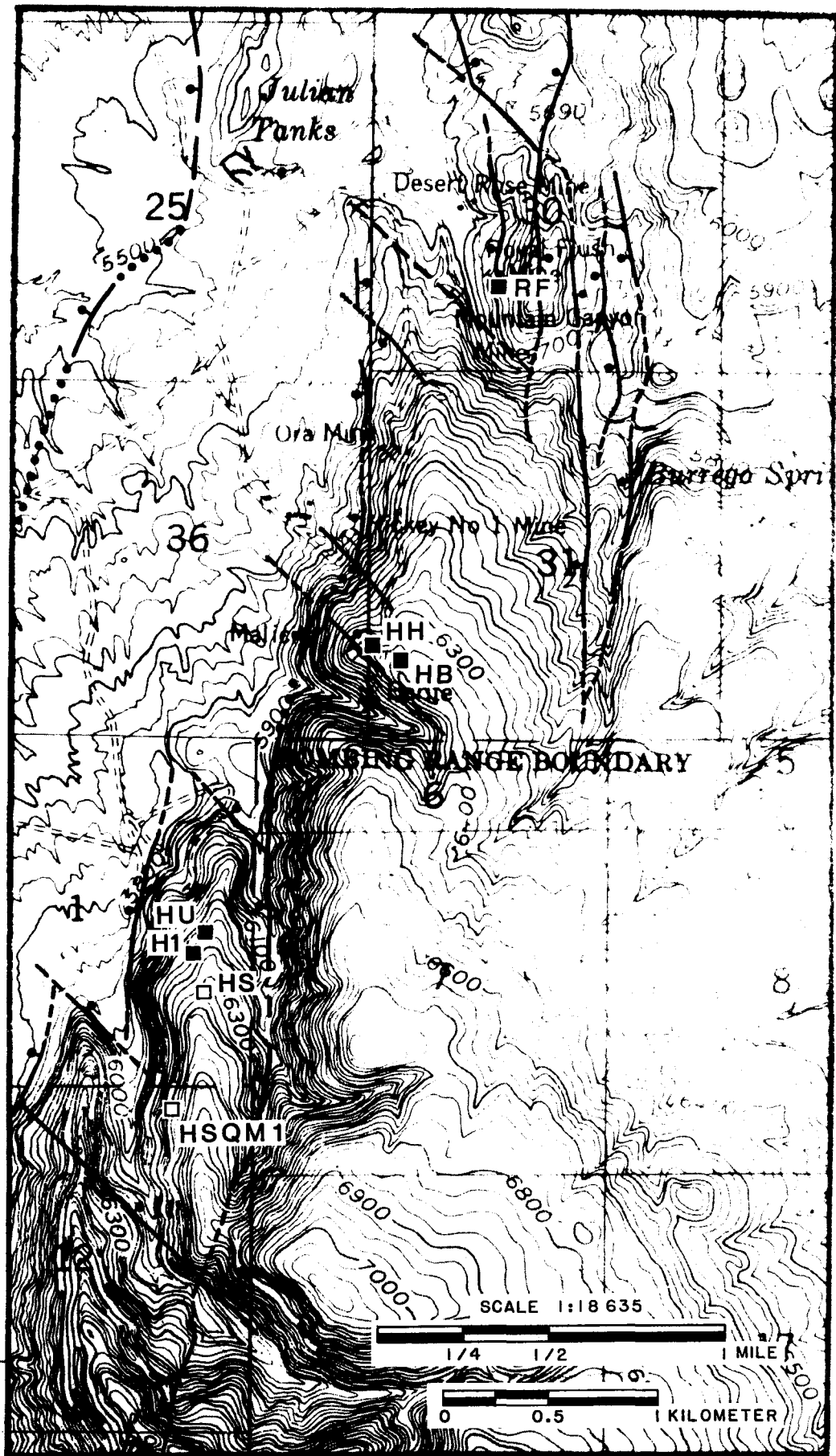


Figure 5

Hansonburg district with major structures,
and sample locations.

Explanation of Sample Location Symbols

Series	Number	Description	Samples
RF	5	Royal Flush	RFG1,2 - Galena RFF1,2 - Fluorites RFFQ1,2 - Quartz
HH	5	Mex-Tex	HHG1 - Galena HHB1 - Barite HHFO,1 - Fluorites TRI - Fluorite HHQ1 - Quartz
HB	4	Barite Mine	HBG1 - Galena HBB1 - Barite HBF1 - Fluorite HBQ1 - Quartz
H1	4	No. 1 Drift	HSPH - Sphalerite H1G1 - Galena H1B1 - Barite H1F1 - Fluorite
HU	4	Sunshine Drift	HUG1 - Galena HUF1-3 - Fluorites
HS	11	Surface	HSG1 - Galena HSB1,2 - Barites HSF1-5 - Fluorites HSQ1,2,3 - Quartz



SAMPLE LOCATIONS AND STRUCTURES

addition to the alignment of igneous features, various structures mark the Capitan lineament. Most prominent are the blunt northern termination of the Carrizozo anticline, and the left-lateral shift in the axis of the Mescalero arch across the Capitan intrusive.

Abrupt termination of structural topographic relief is characteristic of intersections of uplifts with lineaments (C.E. Chapin, 1980, oral. commun.). The Salida lineament in central Colorado marks the northern end of the Sangre de Cristo Range. The Tijeras lineament (Chapin and others, 1979), passing through Tijeras Canyon east of Albuquerque, marks the structural depression between the Sandia and Manzano Mountains, while the Santa Rita lineament causes a similar depression between the Fra Cristobal range and the Caballo Mountains in the southern portion of the state. Similarly, the blunt northern end of the Oscura uplift marks its intersection with the Capitan lineament. These areas of intersection become structurally complex, resulting from the differential uplift across lineaments (Chapin, 1979).

Facies changes within Paleozoic and Mesozoic sedimentary rocks proximal to these lineaments indicate the prolonged activity of these lineaments. Lisenbee et al. (1979) noted marked facies changes and stratigraphic pinching-out in Pennsylvanian strata

across the northeast trending Tijeras-Canoncito fault system, east of Albuquerque. Chapin et al. (1979) noted similar facies and stratigraphic changes in Cretaceous rocks across a structure in the Riley-Puertecito area, southwest of Albuquerque. These two distant features aligned together possessed the same northeast trend demonstrated by the more documented Morenci and Jemez lineaments and were given the name Tijeras lineament (Chapin, 1979). Similar pinching-out of Cretaceous-aged sediments across the Colorado lineament in Colorado has been noted by ~~Davis~~ Weimer (1978).

A paleo-structure was active in south-central New Mexico, being repeatedly uplifted along east-west "hinge" lines during Paleozoic and Mesozoic periods (the New Mexico - Texas arch) (Eardley, 1962; Kelley and Thompson, 1964). A long lived, but perhaps intermittent orogeny climaxed during Pennsylvanian and early Permian-time, and greatly effected the distribution, thickness and lithologic character of those sediments (Wilpolt and Wanek, 1951). Relative to observations from other lineaments, this could mark the involvement of the Capitan lineament in the formation of these uplifts. Differential uplift related to the Capitan lineament may have played a role in the formation of the reef-facies Council Springs limestone.

The facies changes observed within the Council Springs Unit in the Hansonburg district, paired with the thinning of the Paleozoic section in the area (Kottowski, 1960; Kelley and Thompson, 1964) indicate the similarities between this lineament and other lineaments (Weimer, 1978) elsewhere in the western United States.

Ore Deposits

Mineralization

The main-stage hydrothermal mineralization at the Hansonburg deposit consists of galena, Sr-bearing barite (Kopicki, 1963), fluorite, quartz and minor sphalerite (Kottowski, 1953; Roedder et al, 1968; and others). The ore occupies solution cavities and locally, fault breccia (Kottowski, 1953). The ore occurs as discontinuous pods and vugs following solution ways within the karstified Council Springs Unit. Other than silicification, replacement of the limestone is minor and consists of galena and barite.

The mineralized horizons occur in the coarse "rip-up structure" bands of the allochthonous limestone host, while the fine grained beds between rip-up structures are relatively unaffected (Figs. 7,8). Kopicki (1963) described this as "sheeting" which developed parallel to bedding planes to allow access of mineralizing solutions. However there is no indication of forceful injection. Furthermore, the host lithologies present and characteristic of the Council Springs Unit (but previously unrecognized) eliminate the possibility of such a formation.

The mineralization exhibits a layering reflective of the paragenetic history of the ores. This has been described as a banded, or "coontail" ore (Kottowski, 1953; Roedder et al. 1968; and others), after similarly named ores in other Mississippi Valley-type deposits. Vugs of mineralization are often lined by spectacular terminated mega-crystals. In small-scale caverns lined, but not completely filled with mineralization, fluorite will occur only on the floor of the cavern. The fluorite appears to have settled out of the mineralizing fluids onto the floor of the solution cavity, and continued to grow.

The late supergene stage of mineralization is represented by the varietal sulfate, carbonate and hydrate mineral phases of Cu, Pb, Zn, Fe, Ca, and Mg.

Paragenesis

The general paragenesis of the deposit noted by the present author (Fig. 9) is early silicification with replacement of the limestone host by quartz, barite and galena. This is followed by the main-stage open-space mineralization, consisting of galena, barite fluorite and quartz. Sulfide deposition extends from the early replacement stage through some of the later

Figure 6

Hand sample showing minor mineralization
occupying a fissure within the Abo formation
of Permian - age.



Figure 7

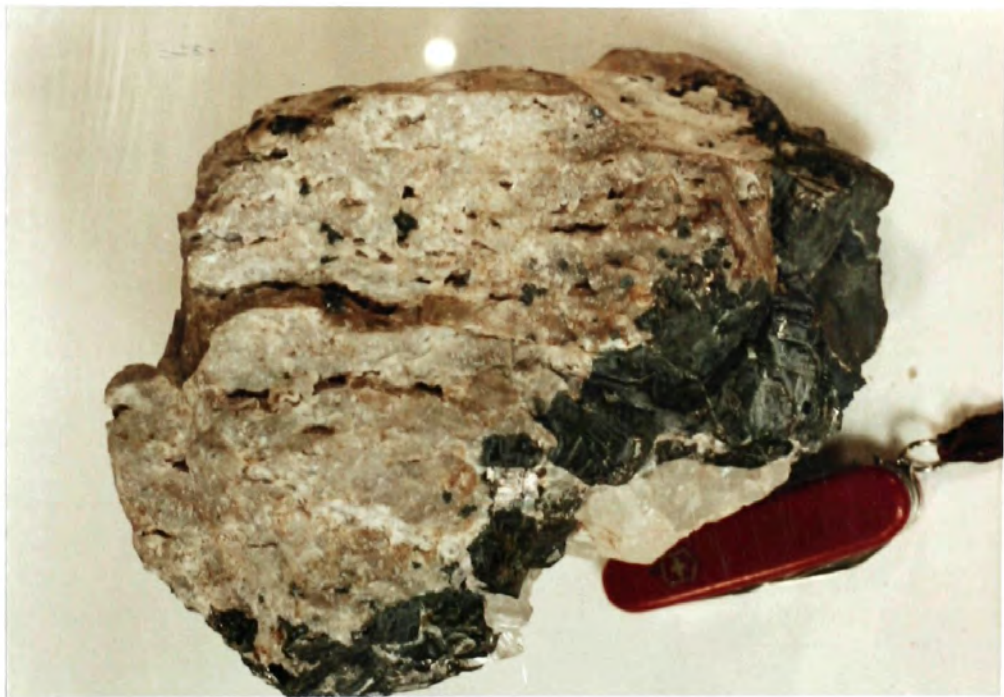
A Examples of unmineralized and mineralized allochthonous limestone. Note excellent correlation between the coarse, fragmental banding and the localization of mineralization. Fine-grained interbeds are relatively unaffected. Extreme lower right edge of the sample nearest the knife is the margin of a large (unmineralized) solution cavity.

B Example of (7A) in the field. Note again the preservation of the fine-grained interbeds.



Figure 8

- A Same unmineralized allochthonous limestone sample shown in Figure 3A.
- B Sample of mineralized limestone showing similarities with 8A. Note massive galena mineralization developed in an adjacent cavity off to the lower right, and the preservation of bedding - plane irregularities in the formation of small-scale horizontal cavities.



phases, with galena predominant, and only minor sphalerite and pyrite. Main stage fluorite deposition commenced post early silicification, though locally all phases seem to have coprecipitated. Minute sulfide inclusions were observed within certain fluorite samples. Grogan and Bradbury (1968, p389) noted similar included sulfides during their discussion of the Cave-in-Rock deposits of Southern Illinois.

Continuous deposition of barite through the paragenesis is indicated by inclusions of barite within sphalerites, fluorites and quartzes throughout the mineralizing event (Fig. 10). However, most barite was deposited later in the mineralizing sequence, and locally completely fills voids. Continuous deposition of silica is indicated (Fig.9) based upon included quartz crystals which were observed in other early mineral phases (eg. sphalerite, early barite, etc.) in agreement Kopicki's ideas (1963, p94). Late silica is characterized by terminated quartz crystals.

Roedder et al. (1968) indicate a paragenesis for the deposit with early "selective replacement" of the limestone host by silica. Resultant unsilicified bands are then leached, dissolved and lined successively with the main stage mineralization assembly of sphalerite, pyrite and galena (early sulfide stage) followed by, and locally precluded by, barite and the many stages of fluorite. Roedder and others (1968)

indicate quartz deposition to be intermittent during other phases, and comprising the final stage of deposition.

Fluorite paragenesis is rather strictly defined by Roedder, based upon coloration and apparent position in the mineralizing sequence. Fluorite is proposed as starting with the early, initial pale-green, nearly rounded variety, to later cubic crystals of a similar pale-green color. Later stages of cloudy, slightly greenish-white cubes are overlain by "limpid-blue" and blue-green varieties successively. Termination of the fluorite phase is marked by a sparse lavender to purple variety, in cubic form.

This study indicates a paragenetic sequence somewhat different from that proposed by Roedder et al. (1968), due in part to increased exposure since Roedder's work. Fluorite coloration showed quite wide variability dependent upon location. The color scheme visible at one site will vary from one cavern to the next, often separated by not more than a few inches of silicified host. For this reason attempts at fluorite paragenesis were found to be ambiguous, and the fluorite is taken to be a single mineral phase regardless of color or its place in the mineralizing sequence.

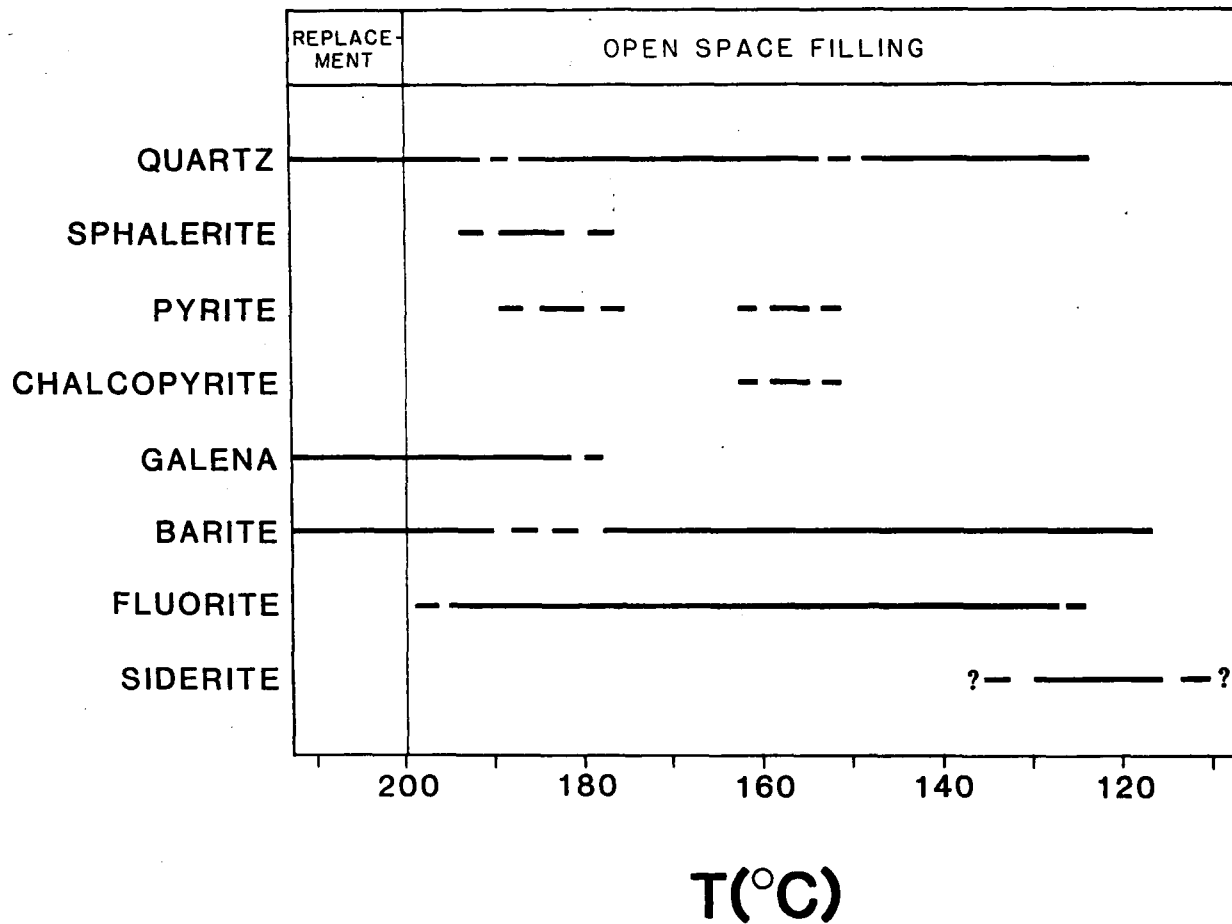
All previous authors reporting on the Hansonburg district have indicated the evidence for possible pulses or surges in the mineralizing system. The solid inclusions observed in this study explain the apparent depositional pulses and continuums observed for a variety of the mineral phases (Fig. 9).

Siderite is present in appreciable amounts locally in the district. Kopicki (1963) indicates siderite's occurrence as joint and vein filling, while occupying a position late in the paragenetic sequence. Roedder et al. (1968) did not address the relative position of siderite deposition in their description of the paragenesis. Siderite was observed primarily in areas void of main-stage hypogene mineralization, as noted by Kopicki (1963). This author proposes therefore, that siderite either represents a separate mineralizing event, or occupies a position late in the mineralizing sequence.

Figure 9

Generalized paragenetic diagram for the mineralization observed at the Hansonburg deposit. Indicated filling temperatures are approximate values based upon inclusion homogenization data.

GENERALIZED PARAGENETIC SEQUENCE



EXPERIMENT

Sampling Procedure

Samples were obtained from six locations along the north-south striking exposure of the mineralization (Fig. 5). Quartz from both early and late mineralizing stages, fluorites of varying color and age, and barite samples were taken at each locality. Sphalerite was sampled from its one located occurrence. The samples were cut and prepared into doubly-polished thick sections for examination (discussed in Appendix C).

Microthermometry was performed utilizing the TH600 heating-freezing stage manufactured by LINKAM Scientific Instruments of London, England. All temperature data were verified by the study of two thick sections (of two different crystals) from each sample. All samples used in these microthermometry determinations, other than the sphalerite samples, were splits of the same samples used in the microanalysis, following.

Fluid inclusions from the samples were extracted and then analysed utilizing various analytical techniques. Twenty-two samples were selected for

analysis based upon the inclusions suitability for extraction and analysis. Galena, fluorite and quartz were analysed. Sphalerite was not found in sufficient amounts to enable analysis. Barite was not analysed.

Fluid Inclusion Study

Types of Inclusions

Over 1200 inclusions from 40 doubly-polished thick sections were studied. Primary, pseudosecondary, and secondary type inclusions were observed. Primary types were quite large, generally greater than 100 microns, and abundant in all minerals examined. Secondary inclusions greatly outnumber other types by almost 100x, however, their size (< 20 microns) is much less than the primary types. Thus, in spite of their greater abundance, the amount of trapped secondary fluid is volumetrically much less than that of the primary inclusions.

The inclusions for the most part were of the simple two phase type (liquid and vapor), with the vapor bubble occupying 1-5% of the inclusion volume. No daughter minerals were found in this study. However, an occasional, minute, highly-birefringent mineral, (as indicated by Roedder et al., 1968, p 341) was seen within some of the samples. This "speck" was not effected by heating or freezing the inclusion (Fig 10-I). Included within some of the primary types from some samples, organic material (after Roedder 1968, p343) was observed, thought its presence did not seem

to affect the heating or freezing behavior of the inclusion. Occasional inclusions appeared to be virtually entirely organics.

One unusual fluorite sample showed "annular-rings" of what appeared to be H₂S (?) (after Roedder, 1971) surrounding the vapor phase during freezing. This ring dissipated into the vapor phase during warming. This sample also contained sulfide inclusions, discussed later.

Microthermometry

In general the results of the fluid inclusion microthermometry studies are similar to Roedder et al., (1968). Homogenization temperatures range from 210-125 C, and salinities from 10-18 eq. wt. percent NaCl (Fig. 11). However, the data from all sample locations are not the same. When plotted against sample locations, a relationship between the data and certain southeast-trending structures can be seen (Fig. 12). Higher filling temperatures and a predominance of early, terminated-quartz crystals proximal to these structures suggest their involvement in the mineralizing activities. Early quartz in locations away from these faults does not develop into terminated crystals.

This early terminated quartz is associated with a very early, lucid green fluorite which also shows high homogenization temperatures (185-200 C) for the initial stages of growth. This is presumed to be the early fluorite (I) discussed in Roedder et al. (1968), though homogenization temperatures of 212 C in accordance with their data were not obtained. This is, however, the "hottest" fluorite from the district (sample HHFO, Fig. 12).

Figure 10 - Fluid Inclusion Photomicrographs

- A,E - Large primary inclusion in fluorite, shown partially frozen (E, RFF2: Th=171, Tm= -13 C).
- B - Primary type containing organic matter (after Roedder et al., 1968) (HUF1: Th=158, Tm= -9 C).
- C - Secondary types, showing necking-down, avoided for microthermometric determinations.
- D - SEM view - showing growth face of quartz crystal. Shape and form of depressions is characteristic of structure.
- D,G - G SEM is cross-sectional view of D. Note characteristic "tooth" shape of growth horizon(s), marked in K by the orientation of included barite crystals (x-nicols, HHQ1).
- F - Primary types in sphalerite, showing necking-down.
- H - Solid quartz inclusion, with resultant primary inclusion located above.
- I - Pseudosecondary (?) type in quartz, showing birefringent speck (HHQ1: Th=179, Tm= -11 C).
- J - Frozen primary in fluorite, showing "annular-ring" of H₂S (?) (HUF2: Th=159, Tm= -7 C).
- N - Oriented solid barite inclusions (X-nicols, HHQ1).
- L - Overall view of abundant solid inclusions (NO x-nicols). Note orientation of quartz crystals (similar to H) pointing upward in growth direction. Long black spines are included sulfides (see text). (Enlargements M,O,P,Q,R,S,T).
- M,P - Tiny isolated sulfide crystals or grains (HUF2).
- Q - Sulfide spine showing similar cross-section to "M" (picture is inverted for comparison purposes).
- O - Spine grown off isolated grain.
- R,S,T - Reflected, transmitted and enlarged reflected pictures of curiously shaped included sulfide crystals. Abundant solid quartz inclusions are also present. Note pyritic-like striations on the growth surface.

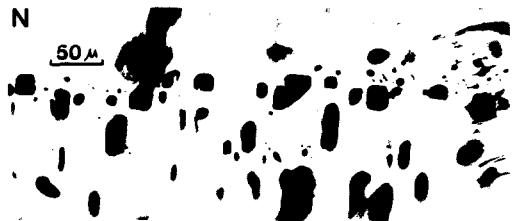
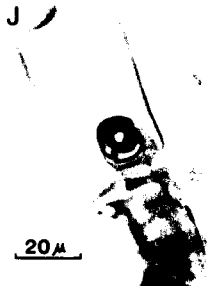
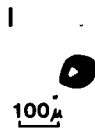
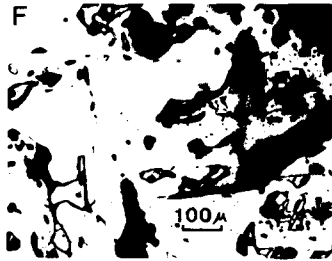
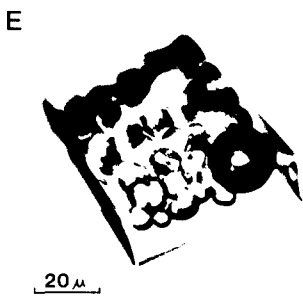
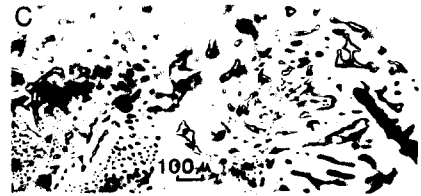
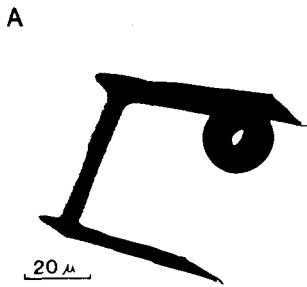


Figure 11

Homogenization and freezing-point depression temperatures plotted against sample location, north to south (left to right). Individual location fields (RF, HH etc.) are plotted in paragenetic sequence, with the earliest mineral phase observed (and its high temperatures) located on the left of each field, and the latest phase observed (with its low temperatures) plotted on the right. HSMQ1 represents a large, multi-stage quartz crystal (6-10 cm.) (see text). A pressure correction of 10-30 C must be added for true formation temperature (Roedder et al., 1968). Dark bars indicate ranges of observed temperatures. Gaps in dark bars indicate groups of data from different growth periods within the same crystal. Higher temperatures were observed at the roots of crystals, with later growth-zones showing cooler temperatures. Thus higher values indicate early growth, while cooler values indicate later growth periods. Dots indicate data from secondary inclusions, connected by lines when ranges were observed.

LAST MELT

T(°C)

-14
-12
-10
-8
-6

HOMOGENIZATION

T(°C)

130
140
150
160
170
180
190
200
210

ROYAL
FLUSH

RF

RFQ1
RFQ2
RFF2

MEX-TEX

HH

HHB1
HHQ1
HHFO
HHF1
TRI

HB

HBFI
HBQ1

HI

HSPH
HIFI

HANSONBURG HILL

HU

HUF3
HUF2
HUF1

HS

HSF4
HSQ2
HSQ3
HSF2
HSF1
HSQ1
HSF5

HSMQ1

130
140
150
160
170
180
190
200
210

10
12
14
16
18

Eq. Wt. % NaCl

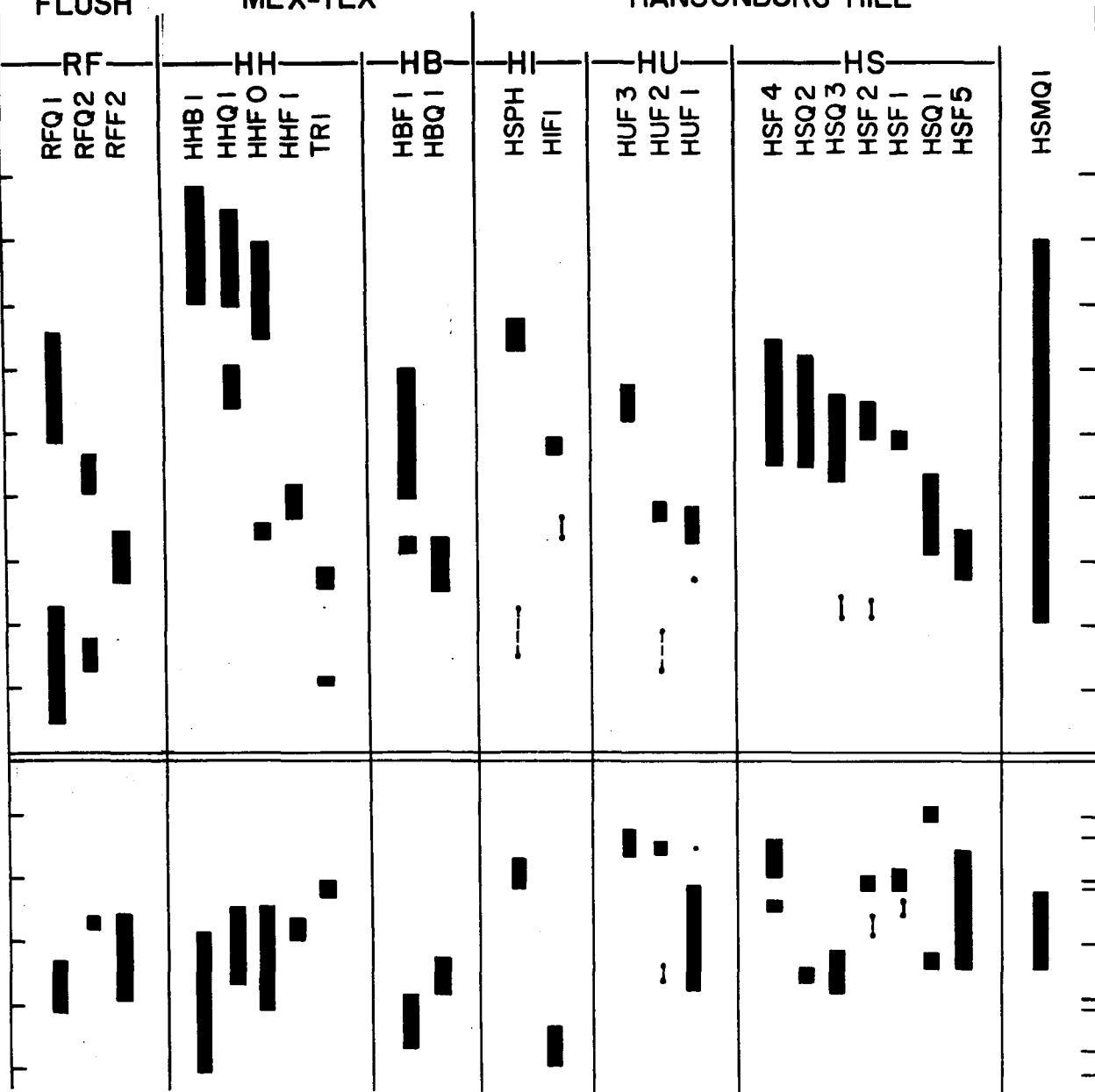
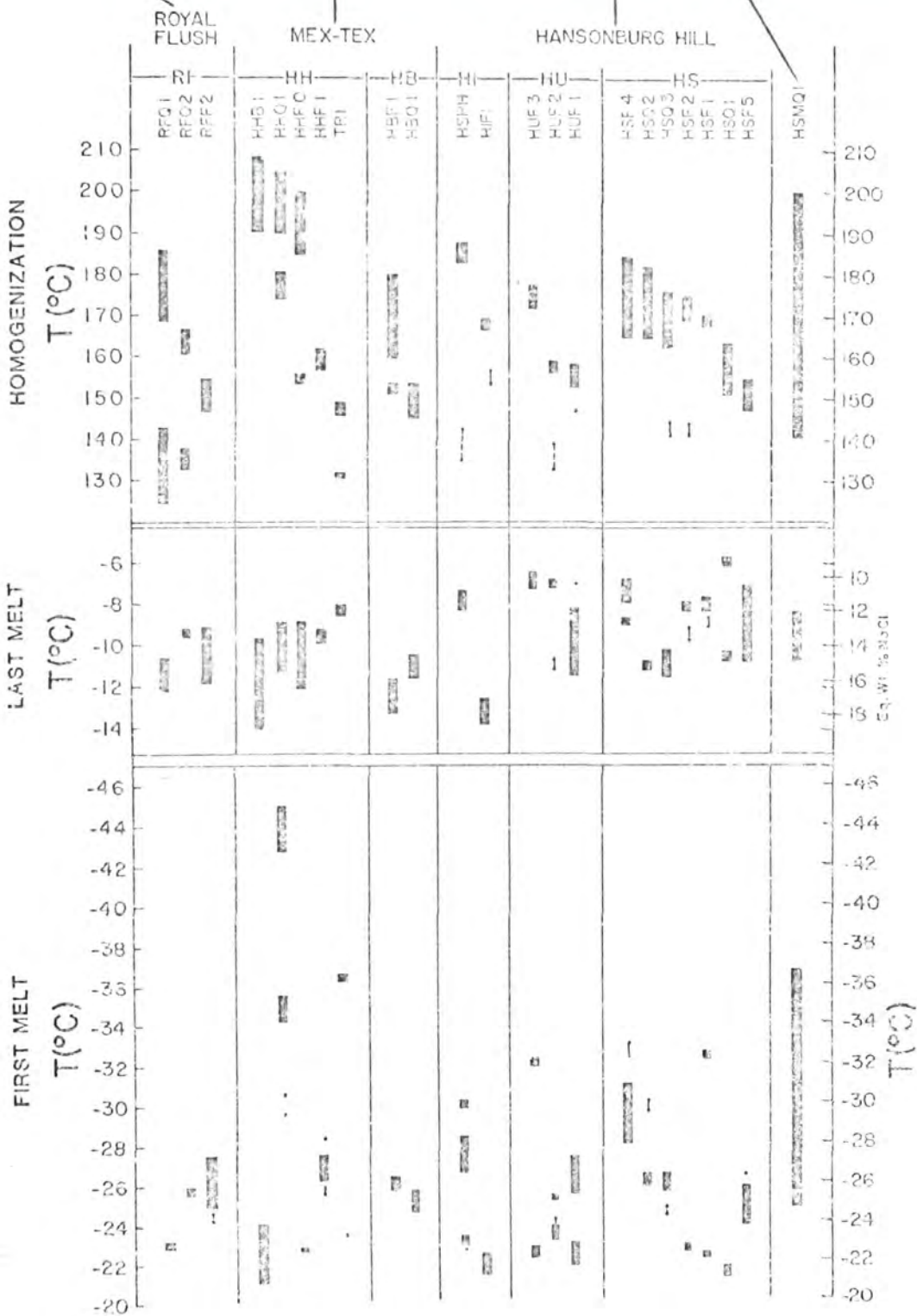


Figure 12

Temperature Data versus Sample Location

Looking toward the Hansonburg site from west in the flats of the Jornada del Muerto, one can see the scar of one of the southeast-trending faults as it bisects the exposed strata. Figure 11, with temperatures of first-melting (first appearance of liquid phase, from completely frozen state), is presented immediately below. Tie-lines indicate sample locations. This diagram exhibits the temperature variations detected relative to the sampling procedure used in this study.



The data from different sample locations all express the same cooling trend for the homogenization temperatures of early to late mineral phases, but do not indicate a district-wide trend. The observed temperatures for HHB1 and HHQ1 resolve the need for Roedder's (et al., 1968) rise in temperature during the fluorite (I) phase. The presence of these high-temperature, early mineral phases indicate variations in the paragenetic sequence not recognized by Roedder et al. (1968), and support the simple cooling of solutions from the initial high temperatures near 200 C. Sample HSMQ1 showed remarkable temperature variations within its growth history, showing also some of the higher temperatures from the district. It should also be noted that within the growth history preserved in HSMQ1 is the same characteristic drop in temperatures of 60 C from early phase to late, as is observed for the deposit's paragenetic sequence as a whole. This sample (HSMQ1), therefore, may represent a complete record of the temperature activity of the mineralizing solutions responsible for the Bingham deposit (Figs. 11, 13).

As opposed to the homogenization data, the observed freezing temperatures do indicate a slight district-wide trend. Salinity values (eq.wt.% NaCl) show an increase toward the north. This study finds

that salinities within distinct locations were locally found to decrease through later mineral phases (Fields: RF, HH, HB and HS(?); Fig. 11, bottom). Roedder et al. (1968) indicated a marked increase in salinity for the later mineralizing solutions, which could not be explained relative to their overall uniform homogenization temperatures (Roedder et al., 1968, p347).

Accompanying the increased temperatures observed at the Mex-Tex local, were very depressed first melting temperatures, particularly in sample HHQ1, which is an early quartz phase (Fig. 12, bottom). First melting temperatures of -44 C were observed, indicating the presence of significant concentrations of CaCl_2 , as neither NaCl nor KCl can produce this great a depression (Konnerup-Madsen, 1979, Figure 1, p13). Increased dissolution of the carbonate host proximal to these structures would explain this calcium increase.

Suitable primary inclusions for microthermometry measurements in barite proved to be very sparse, surely less than 1% of all inclusions observed. On the few samples examined before discontinuing study of this species (due to the lack of suitable inclusions for extraction and analysis) this author noted a very narrow range of homogenization temperatures (18 C) from 208-190 C, indicating earlier, high temperatures. This

reflected barite's early position, as observed, in the mineralizing sequence. Solid phase quartz crystals were observed extensively within the barite.

Roedder et al. (1968, p343) reports that there is abundant evidence of leakage of inclusion fluid during heating of barite, and indicates homogenization temperatures over a 74 C range (173-99 C). They feel that the temperatures toward the lower end are more representative, indicating cooling during the later stages of mineralization.

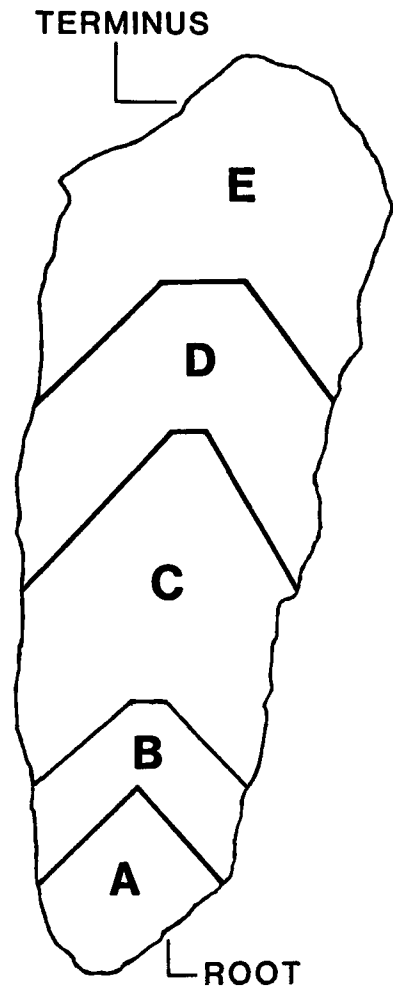
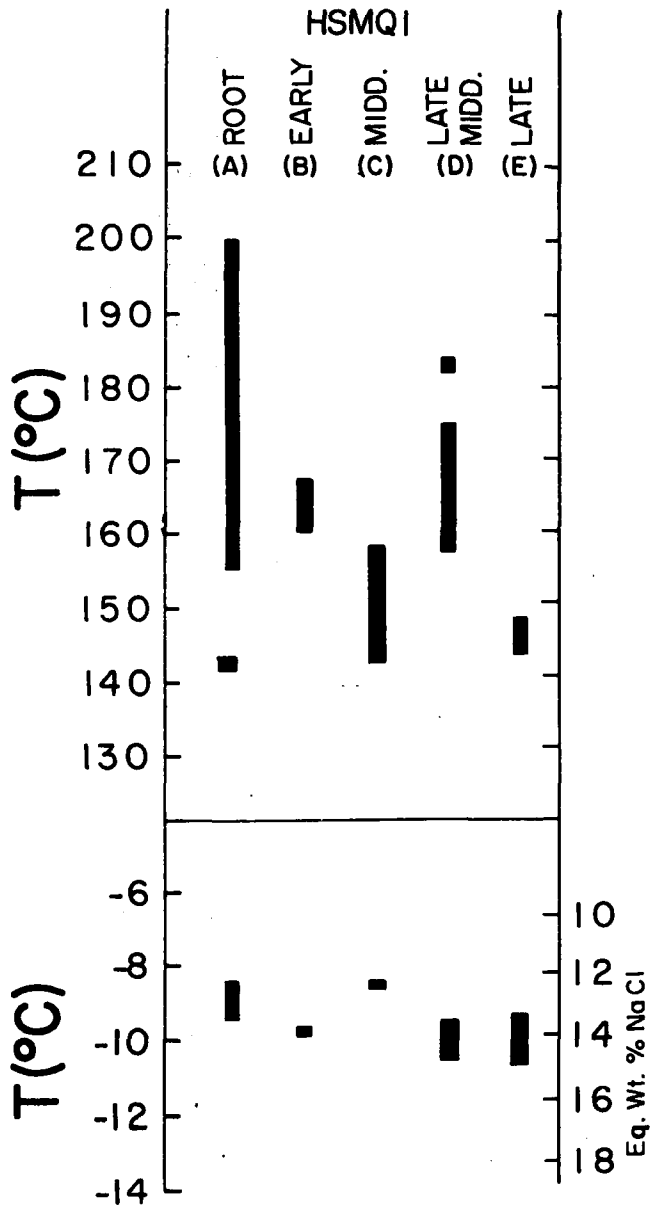
Allmandinger (1975) reports homogenization data from apparent pseudosecondary inclusions in barite, with a temperature spread of 137 C (217-70 C). The wide range of temperature indicates either extensive leakage during homogenization, or confusion over inclusion types. Of interest, however, is the very wide range of temperatures observed, and the gaps separating the groups of data. This indicates that perhaps Allmandinger's observations included some primaries of the type identified by this author, which yield temperatures over a narrow range, are separated from all others by almost 45 C, and indicate temperatures of 212-217 C, representing an early temperature of formation.

Figure 13

Quartz Sample - HSMQ1

Growth Zone	Data and Period Represented
A	T - highly variable (212-140 C). Initial entrance of mineralizing solutions - major tectonic dislocation?
B	T - stabilized to narrow range (180-170 C). Solid barite visible along slight growth boundary.
C	T - continues to drop, maintaining narrow range (160-150 C). Abundant trash between slight growth zones - debris from structural activity?
D	T - increased 20 C, but remains over narrow range - slight reentrance of mineralizing solutions?
E	T - drastically reduced (150-140 C). Tip or terminus zone of crystal - lack of primary inclusions (slow steady growth?).

Cross-section Sample HSMQ1



(1.9x)

Scanning Electron Microscopy

Since analyses of inclusion fluids is the major part of this study, crushed samples were examined by SEM to determine: 1. Location of dehydration products upon release from the inclusions. 2. Quantitative compositions of dehydration products, and 3. Quantitative compositions of sulfides included within certain fluorites. Crystals were cleaved, shattered or otherwise opened, exposing the inclusion's contained fluid and vapor phases to the atmosphere. Surrounding and locally within the inclusions that are intersected by the plane of fracture will be found both dehydration products of the liquid phase, and daughter minerals if any were present before fracture.

Dehydration products when found in this study were predominantly sodium and calcium chlorides, and occasional potassium chlorides. For the most part these dehydrates were spilled from within the inclusion void or perched upon the lip of the inclusion. This is the result of very rapid dehydration of the minute liquid volumes upon exposure to room temperature and pressure. Occasionally, though commonly with the galenas where enough water is present, the dehydrated halite crystals will be spilled onto the fracture

surface and will spread laterally, exhibiting epitaxial growth aligned with the fabric of the galena (Fig. 15 A,D,G). Head (1932) noted similar occurrences in galenas from the Joplin (Tri-state) district.

Morphologies of the sulfides in fluorite are tetrahedra, cubes (Fig. 15 E,F) and spines. X-ray analysis indicates the presence of varying amounts of iron and sulfur, with minor copper, lead, and zinc. The sulfide inclusions have a variable elemental content. This would explain the wide diversity of crystal shapes observed (Fig. 10 L,M,O-T). These sulfides appear to be predominantly pyrite and chalcopyrite.

Figure 14

Scanning Electron Microscope Photomicrographs

- A,B - Large, fractured primary inclusion in galena and quartz, showing dehydration products spilling out of inclusion void.
- C - Large, fractured primary inclusion in fluorite, with "massive" dehydration products remaining in void (halite - note shape; and sylvite).
- E - Enlargement of A. Note epitaxial growth of halite crystals, oriented with fabric of galena.
- G - Overall view of A and D. Note abundant clusters of oriented halite crystals (small, in background).
- E,F - Fluorite with sulfide inclusions. Note cubic shape in F.
- H,I - Enlarged views of F. I is a map of iron and sulfur, by X-ray analyzer. Note excellent correlation.



5 μ

20 μ

40 μ

10 μ

20 μ

20 μ

50 μ

Microanalytical Determination

Cleaning and Extraction Procedures

Sample cleaning and fluid extraction procedures closely followed the methods described by Roedder et al. (1963) and Rye and Haffty (1969), with only one major exception. Inclusion fluids are released by crushing the samples in a pre-cleaned, type 304 stainless steel tube under vacuum. The inclusion fluids vaporized upon exposure to vacuum, and were frozen and trapped using a liquid nitrogen bath. Pressure readings taken while using the liquid nitrogen indicate the presence of non-condensable gasses (H₂S, CH₄ etc.). None were detected during this study. Replacing the liquid nitrogen bath with a slurry of dry-ice and acetone, which allows the vaporization of the frozen CO₂ but not the frozen H₂O, enables the measurement of CO₂ pressure. Removal of the dry-ice and acetone slurry vaporized the frozen H₂O, which was then frozen into a pre-weighed capillary, and weighed.

Leaching Procedure

Distilled, doubly-deionized water was used for all leaching solutions. This water (pH 4.9 - 5.4) was continually analysed through the course of the study to insure that purity was being maintained. This water contained virtually undetectable amounts of the ions of interest in this study.

Samples that have been crushed were poured out of the stainless steel tube into a precleaned Teflon beaker which contained 20 ml leach water. The stainless-steel tube was discarded. Roedder et al. (1963) and Rye and Haffty (1969) rinsed out the stainless-steel extraction tubes with ultra-clean leach water, adding the rinse solution to the total leach volume. Tubes were not rinsed during this study for it was found during preliminary blank runs, that Fe, Cu, Zn, Ca and F were being leached from the walls of the tube. The problem of contamination from the tubes was eliminated upon removal of this step. The crushed material was allowed to soak in the Teflon beaker for 10-20 minutes, and the supernatant liquid was then decanted into a "filter-vac" set up for retrieval of the filtrate, or leach solution. This decantation procedure was repeated 4-5 times.

Once sufficient decantate exists, it is poured off and stored in tightly capped linear polyethylene bottles, which have been precleaned and then rinsed with 2-4 rinses of leach water.

It is preferable to keep minimized the total volume of leach solution, as an increased volume is equivalent to increased dilution factor, making minor elements difficult to detect. However, while keeping the leach solution to a minimum volume one must be certain to use sufficient water and time, to be certain that all water soluble species are extracted from the crushed material.

Roedder et al. (1963) utilized a conductivity meter for this purpose, monitoring the relative amount of dissolved ions. In this study preliminary runs were performed, using prepared "sample" solutions which delineated the procedures to be followed for actual extractions.

Atomic absorption spectrophotometry was utilized for analysis of cations. The hollow graphite furnace (HGA) was employed for copper, iron, lead and barium. The solutions were entered onto the HGA furnace in aliquots of 1,10,20,50 and 100 microliters via Beckman micro-pipets. This method allows for sensitivities of up to 5 micrograms per liter solution. Other cations were measured using the open-flame technique, being

aspirated directly into the flame. Instrument conditions used were those specified by the manufacturer.

Specific-ion electrodes were utilized for determination of both chloride and fluoride ions, allowing for extreme sensitivities of 10^{-6} (M) and 10^{-7} (M) respectively. A turbidimetric method was employed to measure sulfate concentration. Minimum detectable concentrations of sulfate by this method are 1 milligram per liter (1ppm) in accord with other methods.

Blanks

Blanks of two different types were utilized in this study. The first type was a series of blanks consisting of quartz-rod and small, sealed capillaries containing known volumes of leach water. The second type of blanks consisted of quartz rod and similar capillaries which contained known amounts of analysed brines. Twenty to thirty grams of quartz-rod was used in each blank. Blanks were put through the extraction procedure in the same manner as were the samples, and comprised 45% of all the samples run in this study.

The use of the quartz-rod enabled the simulation of both the surface area of the sample generated by crushing, and the maximum deformation to be expected of the stainless steel tube from the crushing of the actual samples which was to follow.

The results of the analyses run on blanks indicate only minor contamination problems (Table I). Generally, background contaminants are considerably less than the amounts of anions and cations in leach-solutions from the crushed mineral samples. The levels of contaminants detected within all blanks were averaged and then subtracted from the corresponding ion for each sample, yielding the corrected and actual chemistry for each sample.

Artificial Inclusions

In this study preliminary runs were performed using micro-amounts of prepared brine solutions which were sealed in cleaned, 3mm capillary tubes and placed in extraction tubes along with cleaned quartz rod. The solution entered into the capillary tubes was prepared in such a way as to approximate those concentrations reported from other fluid inclusion analysis (Hall and Friedman, 1963, and others).

The extraction of these known solutions indicated to what extent the inclusion extraction process was effective. The results of these determinations (Table I) indicate very effective extraction.

TABLE I. ANALYSIS OF BLANKS

Sample No.	Ca (ppm)	Mg (ppm)	K (ppm)	Na (ppm)	Zn (ppm)	Cu (ppm)	Pb (ppm)	Fe (ppm)
BL-III	.02	.00	.02	.05	.05	6.0	4.5	1.5
BL-IV	.06	.00	.00	.07	.07	5.0	5.0	.20
BL-V	.05	.00	.00	.02	.02	ND	ND	ND
BL-VII	.00	.00	.00	.03	.01	ND	ND	ND
BL-VIII	.00	.00	.00	.03	.01	ND	ND	ND
BL-IX	.02	.00	.00	.02	.03	ND	ND	ND
BL-X	.01	.00	.00	.02	.03	ND	ND	ND
BL-XII	.01	.00	.02	.07	.03	ND	5.0	ND
BL-XIII	.01	.00	.00	.04	.00	ND	5.0	ND

ANALYSIS OF ARTIFICIAL INCLUSIONS

Solution A	.38	.17	.27	3.09	.09	.05	.01	.05
Solution B	3.32	.18	.53	2.93	.16	.12	.03	.10
Total	3.70	.35	.80	6.02	.25	.17	.04	.15
BL-VI*	3.81	.27	.86	5.67	.23	.15	.09	.20
		77%		94%	92%	88%		

ND = None Detected

* = BL-VI contained sealed capillaries (2) with solutions A,B -
 Values corrected for background (Ave., BL-III — BL-XIII, above).

COMPOSITION OF FLUID INCLUSIONS

Analyses of fluid inclusion waters are presented in Tables II and III. Cation to anion balances indicate insufficient anions relative to the amounts of detected cations (Table III). The lack of SO₄ values, (and Ba) could relieve, perhaps some of this imbalance (see SO₄= discussion, following). Because of the relatively poor sensitivity of measuring sulfate, the solutions could have contained from 0.1-0.4 molal SO₄ without being detected. As in the analyses from other Mississippi Valley-type deposits, Cl values are not in sufficient amounts to account for all cation complexes.

Fluorine values have not been reported in analytical studies of the fluid chemistry of other Mississippi Valley-type deposits. However, this study indicates F levels of 500-1000 ppm. Sr was not analysed in this study, though Kopicki (1963) indicates its ubiquitous association with faults in the district. This relation seems to indicate access ways utilized by the mineralizing solutions, as Sr is not present in appreciable amounts within the sediments (Kopicki, 1963).

Mineral solubilities annulled the values of those ions which composed the involved mineral. Pb and SO₄ values could not be ascertained from the galena

samples, and similarly, Ca and F values could not be discriminated in fluorite analyses.

Both fluorite and quartz phases show appreciable amounts of metals, commonly ranging up to 2000 ppm, though notably high metal values occur sporadically throughout Table II. In fluorites the values are quite anomalous, while in quartz the values are not so obviously anomalous. Fluorite sample HUF2 shows 1,000 ppm copper, and is the sample which contained the sulfide (cpy.) inclusions. The high Pb values in the two fluorites can not readily be explained.

Observations of uncleaned quartz samples on the SEM indicated the presence of Fe, Pb, and Cu oxides and sulfides within internal growth boundaries. Similar observations of cleaned samples (as those used for extraction and analysis) showed nothing. Thus these anomalous values are not easily understood. It is felt by this author that the metal values did not change drastically during mineralization, and are similar to those values found in the galena and fluorite phases.

The fluid inclusion waters in minerals from the Hansonburg district are characterized by Na-Ca-K Cl brines. Galena phase fluids are somewhat more concentrated than the other fluids. K/Na ratios were found to decrease from the galena through the later phases, while Ca/Na ratios remained stable, and the

Cl/Na ratios, after a initial decrease from the galena phase (reflective of the high Cl values), increased slightly from the fluorite to late quartz phases.

Na/K filling temperatures were calculated using Norman's (1977) modification of Fournier and Truesdell's Na-K-Ca geothermometer. The results indicate excellent agreement between measured fluid inclusion homogenization temperatures for the fluorite and quartz phases and calculated values (Fig 15). Agreement between temperature calculations from Na/K ratios and fluid inclusion measurements strongly suggest that the temperature calculations for the fluids in galena and barite accurately represent depositional temperatures for those phases.

The chemistry of the Hansonburg inclusion fluids is remarkably similar to those values reported from other Mississippi Valley-type deposits (Table V). Sulfate concentrations were not detected in this study, other than those levels resultant from sulfide mineral solubility (PbS). Paired with this low SO₄ concentration is the notable lack of Ba values. All samples were analysed for Ba, though none was detected. It is felt by this author that even though barite is one of the more prevalent mineral species in the Hansonburg district, SO₄ and Ba are in concentrations below the limit of analytical detectability for the

procedures used in this study. The extremely low solubility for BaSO₄ (K_{eq} -BaSO₄ = 10 (exp) ^{-9.76}, at 200 C - Helgeson, 1969), suggest that any Ba or SO₄ in solution would readily combine and precipitate barite. This would result in the decrease of each species concentration level in solution.

TABLE II. FLUID INCLUSION COMPOSITIONS

Sample No.	Weight Extracted H ₂ O (μ g)	Dilution Factor	SOLUTION COMPONENTS										TEMPERATURE (°C)	
			Ca (ppm)	Mg (ppm)	K (ppm)	Na (ppm)	Zn (ppm)	Cu (ppm)	Pb (ppm)	Fe (ppm)	Cl (ppm)	F (ppm)	Calc T _h (Na/K) ²	Meas. T _h (Ave.)
HSQ1	18.8	5,100	5,700	<40	3,680	36,700	260	<10	*	70	51,060	720	211	-
HUG1	18.0	4,400	8,900	<40	4,040	42,400	1,700	<10	*	166	79,020	1,980	207	-
HBG1	20.0	4,600	5,460	320	8,870	58,380	230	<10	*	40	127,400	910	242	-
HEG1	17.3	4,000	16,680	40	3,470	32,920	520	<10	*	140	51,870	800	218	-
RFG1	(NR)	(4,400) ¹	5,500	40	9,000	87,000	180	<10	*	120	168,720	220	213	-
HSF1	1.4	47,900	*	<40	1,440	45,950	<50	140	3,490 ⁺	<10	22,970	*	142	170
HSF2	4.7	12,600	*	130	1,630	36,140	130	120	251	110	17,700	*	166	174
HSF5	3.2	23,400	*	4,920	3,990	96,340	<50	310	280	40	33,050	*	158	147
HUF1	7.4	8,800	*	<40	2,280	36,700	<50	120	325	570	28,100	*	176	155
HUF2	4.0	14,800	*	150	1,620	37,470	<50	1,060 ⁺	840	430	19,180	*	164	158
H1F1	4.4	17,300	*	<40	2,420	47,840	<50	670	22,110 ⁺	100	24,350	*	170	168
HHF1	7.3	10,000	*	<40	1,600	39,800	<50	20	340	800	32,000	*	161	160
RFF1	8.1	8,600	*	<40	1,380	28,600	<50	50	10	2,680	18,140	*	167	
RFF2	8.0	9,100	*	<40	2,000	37,050	<50	110	580	680	20,080	*	176	147
HSMQ1-II _A	(NR)	(19,700) ¹	3,940	<40	1,970	44,790	790	280	650	1,220	38,470	550	164	120-149 ³
HSMQ1-II _B	(NR)	(30,500) ¹	3,360	<40	1,220	68,720	610	700	2,530	100	50,390	1,010	122	142-200 ³
HSMQ1-I	3.7	26,200	2,880	<40	3,410	58,460	49,290 ⁺	920	5,300 ⁺	2,200	65,540	<520	178	120-200 ³
HSQ3	5.7	17,000	25,700 ⁺	<40 ⁺	510 ⁺	15,320 ⁺	510 ⁺	1,200 ⁺	12,930 ⁺	740 ⁺	20,420 ⁺	3,740 ⁺	127	174
HSQ2	6.1	13,900	4,590	<40	2,640	38,500	4,590 ⁺	6,640 ⁺	500	2,430	58,380	<140	150	165-180 ³
HEQ1	5.3	26,400	2,380	530	790	32,500	260	1,890	12,830 ⁺	1,300	36,960	<530	124	148
EEQ1-II	5.0	14,800	2,660	<40	1,040	36,260	290	2,870	14,280 ⁺	100	25,160	270	139	148
HHQ1	8.0	17,500	3,680	<40	1,230	48,480	2,100	360	2,940	650	73,500	<180	138	158

"- " = None Measured

* = High Concentrations due to Mineral Solubility

NR = No Recovery

1 = Estimated

2 = Norman (1977)

3 = Ranges of T_h Measurements Indicate Presence of more than one growth phase

G = Galena

F = Fluorite

Q = Quartz

+ = Not Used, Due to Possible Contamination

HS = Hansonburg - Surface

HU = Hansonburg - Underground (Sunshine Drifts)

H1 = Hansonburg - "No. 1" Drift

HB = Hansonburg - "Barite Mine" Local

HH = Hansonburg - "Mex-Tex" Local

RF = Hansonburg - Royal Flush Local

HSMQ1-I = Composit Sample

HSMQ1-II_A = Terminus Zone of CrystalHSMQ1-II_B = Root Zone of Crystal

TABLE III. FLUID INCLUSION COMPOSITIONS

Sample No.	VOLATILES							molality $\frac{M_{CO_2}}{KgH_2O}$	SOLUTION COMPONENTS							
	Weight Extracted H ₂ O (μ g)	Moles H ₂ O ($M \times 10^{-4}$)	ΔP CO ₂ (extraction) line (mm Hg)	Atm CO ₂ ($\times 10^{-4}$)	Moles CO ₂ ($M \times 10^{-6}$)	Mole % CO ₂ (%)			Molality				Atomic Ratios			
								Ca	Mg	K	Na	Cl	K/Na	Ca/Na	Cl/Na	Cation/Anion** (milliequivalents)
ESG1	18.8	10.4	.228	3.56	1.91	.18	.10	.17	<.001	.11	1.90	1.71	.06	.09	.90	1.34
HUG1	18.0	10.0	.525	8.20	4.41	.44	.24	.26	<.001	.12	2.20	2.65	.05	.12	1.20	1.03
HBG1	20.0	11.1	.460	7.19	3.87	.35	.19	.16	.016	.27	3.02	4.27	.09	.05	1.41	.85
HHG1	17.3	9.61	.518	8.09	4.35	.45	.25	.50	.001	.11	1.71	1.74	.06	.29	1.02	1.57
RFG1 ¹	(NR)	-	.470	7.34	3.95	-	-	.16	.001	.27	4.51	5.66	.06	.04	1.25	.90
ESF1	1.4	.778	.147	2.30	1.24	.16	.10	*	<.002	.04	2.22	.72	.02	*	.32	*
ESF2	4.7	2.61	.125	1.95	1.05	.40	.22	*	.006	.05	1.75	.55	.03	*	.31	*
HSP5	3.2	1.78	.097	1.52	.817	.46	.26	*	.225	.11	4.66	1.03	.02	*	.22	*
HUF1	7.4	4.11	.093	1.45	.780	.19	.11	*	<.002	.06	1.77	.88	.03	*	.50	*
HUF2	4.0	2.22	.108	1.69	.909	.41	.23	*	.007	.05	1.81	.60	.03	*	.33	*
H1F1	4.4	2.44	.290	4.53	2.44	1.0	.56	*	<.002	.07	2.31	.76	.03	*	.33	*
H2F1	7.3	4.06	.405	6.32	3.40	.84	.47	*	<.002	.05	1.92	1.00	.03	*	.52	*
RFF1	8.1	4.5	.498	7.78	4.18	.93	.52	*	<.002	.04	1.38	.57	.03	*	.41	*
RFP2	8.0	4.44	.298	4.66	2.51	.57	.32	*	<.002	.06	1.79	.63	.03	*	.35	*
HSMQ1-II _A ¹	(NR)	-	-	-	-	-	-	.11	<.002	.06	2.19	1.23	.03	.05	.56	2.0
HSMQ1-II _B ¹	(NR)	-	-	-	-	-	-	.09	<.002	.04	3.36	1.59	.01	.03	.47	2.16
HSMQ1-I	3.7	2.05	.143	2.31	1.24	.60	.33	.08	<.002	.10	2.86	2.07	.03	.03	.72	1.47
HSQ3	5.7	3.17	.150	2.34	1.26	.40	.22	.72	<.002	.01	.75	.65	.01	.96	.87	2.5
HSQ2	6.1	3.39	.250	3.91	2.10	.62	.34	.13	<.002	.08	1.88	1.85	.04	.07	.98	1.2
HBQ1	5.3	2.94	.115	1.80	.968	.33	.18	.07	.025	.02	1.59	1.17	.01	.04	.74	1.5
HBQ1-II	5.0	2.78	-	-	-	-	-	.07	<.002	.03	1.77	.80	.02	.04	.45	2.4
HHQ1	8.0	4.44	.20	3.13	1.68	.38	.21	.10	<.002	.04	2.37	2.33	.02	.04	.98	1.1

NR - No Recovery

¹ - Concentration (m) estimated

* - High Concentration Due to Mineral Solubility

** - Includes F values (not shown)

SAMPLE CODE - TYPE

G - Galena

F - Fluorite

Q - Quartz

SAMPLE CODE - LOCATION

HS = Hansonburg - Surface

HU = Hansonburg - Underground ("Sunshine" Drifts")

H1 = Hansonburg - Underground (No. 1 Drift)

HB = Hansonburg - "Barite Mine" Local

HH = Hansonburg - "Mex-Tex" Local

RF = "Royal Flush" Local

TABLE IV. AVERAGED LOG VALUES OF FLUID INCLUSION COMPOSITIONS (ppt)
WITH 90 PERCENT CONFIDENCE LIMITS

	Ca	Mg	K	⁴⁰ K/ ²³ Na	Na	Zn	Cu	Pb	Fe	Cl ⁻	F ⁻
GALENA											
\bar{X}	.88	-1.22	.72	.45	1.68	-.40	-	*	-1.02	1.93	-.13
S	.21	.40	.21		.17	.39	-	*	.25	.23	.34
S ₉₀	.19	.36	.19		.15	.35	-	*	.23	.21	.31
FLUORITE											
\bar{X}	*	-1.05	.29	.18	1.63	-1.25	-.81	-.49	-.67	1.37	*
S	*	.69	.15		.15	.14	.53	.72	.76	.10	*
S ₉₀	*	.43	.09		.09	.09	.33	.48	.47	.06	*
QUARTZ											
\bar{X}	.52	-1.24	.19	.11	1.66	-.08	.05	.22	-.18	1.67	-.43
S	.10	.42	.23		.12	.49	.50	.44	.59	.16	.31
S ₉₀	.07	.31	.17		.09	.40	.37	.42	.43	.12	.23

\bar{X} = Arithmetic Mean

S = Standard Deviation

S₉₀ = 1/2 Range, Standard Deviation, at 90% Confidence Level

"+" values (Table II) not used

* = High Concentrations due to Mineral Solubility

- = None Detected

Figure 15

Ranges of Calculated (Na/K) and Measured Temperatures

Calculated Na/K temperatures were arrived at by the following relation:

$$1000/T(K) == A \log (Na/K) + C$$

where: Na and K are in molar amounts, and A and C are the coefficients used for a least squares fit.

$$A == .6782 (\pm .0204)$$

$$C == 1.2280 (\pm .0262)$$

(Norman, 1977)

RANGES OF CALCULATED (Na/K) AND MEASURED TEMPERATURES

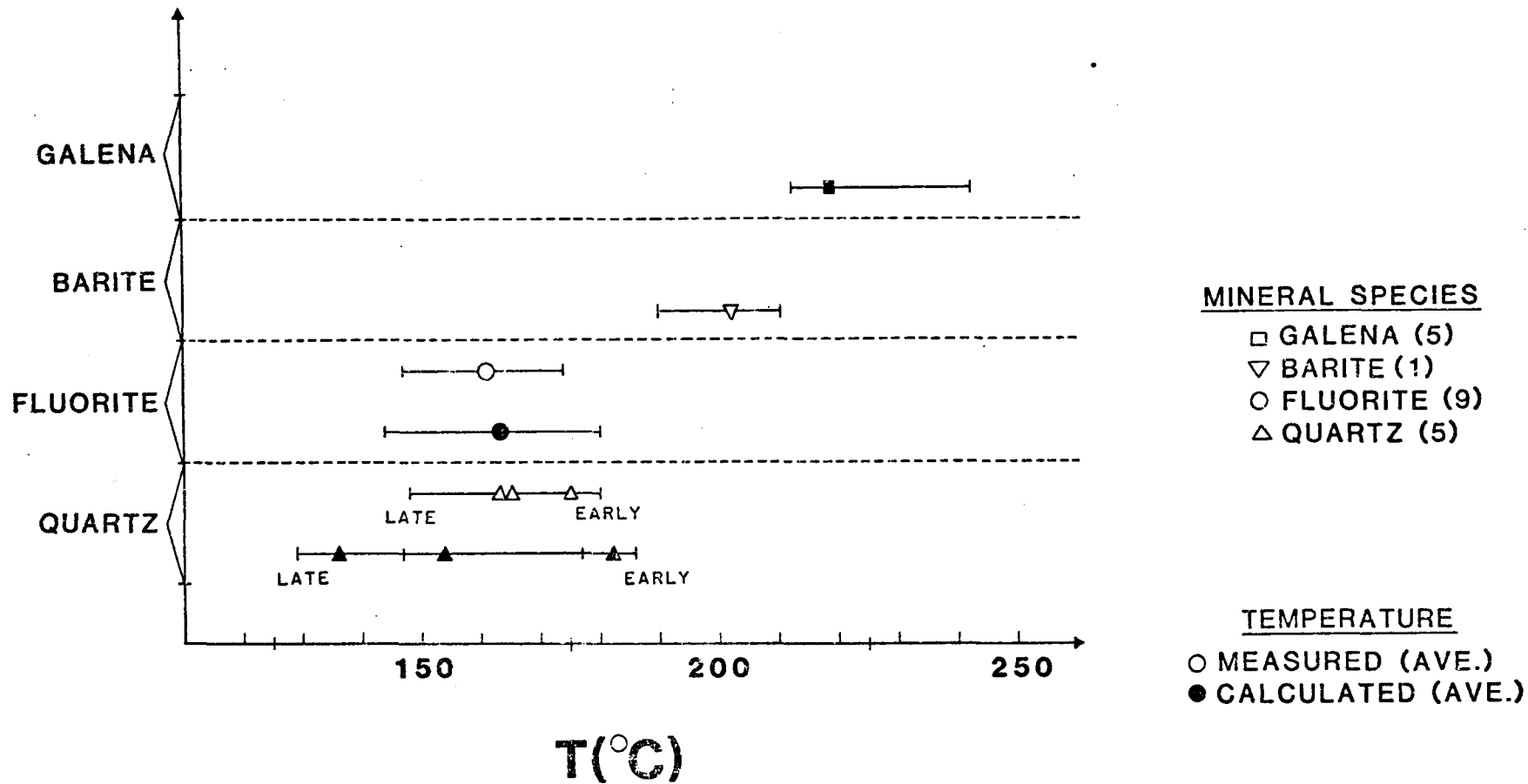


TABLE V. COMPARISON OF HANSONBURG ANALYSES, TO THOSE OF OTHER MISSISSIPPI VALLEY TYPE DEPOSITS, AND PRESENT DAY FORMATION WATERS

	Ca (ppm)	Mg (ppm)	K (ppm)	Na (ppm)	Cl (ppm)	F (ppm)	SO ₄ (ppm)
GALENA							
Cave In Rock ¹	20,600	4,000	3,100	55,400	115,000	NR	*
Wisconsin-Ill. ¹	18,500	3,400	3,200	39,000	83,000	NR	ND
Hansonburg	7,600	60	5,300	47,900	85,100	700	≤8 ⁴
FLUORITE							
Cave In Rock ¹	*	4,500	3,000	44,200	90,900	NR	3,200
Cave In Rock ^{2A}	*	5,600	4,800	64,600	127,100	*	17,400
Cave In Rock ^{2B}	*	3,600	2,900	39,500	78,400	*	7,900
Hansonburg	*	90	2,000	42,700	23,400	*	≤30 ⁴
QUARTZ							
Cave In Rock ¹	8,400	2,800	4,300	17,300	47,000	NR	12,900
Hansonburg	3,300	60	1,600	45,700	46,800	400	≤30 ⁴
FORMATION WATERS ³							
Beula Simon	2,900	250	460	29,800	54,400	NR	380
Pleasant Bayou	8,700	650	550	36,300	79,100	NR	<5
Fairfax-Foster-Sutter	5,500	640	820	43,700	91,900	NR	<5

¹ Hall and Friedman (1963)

^{2A} Roedder, Ingram and Hall (1963) - Extracted H₂O

^{2B} Roedder, Ingram and Hall (1963) - Visual Estimate of H₂O

³ Randolph et al. (1980)

⁴ Calculated Maximum from Anhydrite Equilibrium

Thermodynamic Calculations

All calculations regarding the various mineral species utilized the averaged analytical data, Table IV and the equilibrium constants in Appendix I, Table II. Fluorite analyses were excluded from the majority of the calculations due to the lack of Ca values. A version of the PATH (Helgeson et al., 1970) computer program used at New Mexico Institute of Mining and Technology was applied to the data. PATH results are shown on figures and described at the end of this section.

Ionic Strength

The ionic strength of the mineralizing solution(s) responsible for the Hansonburg deposit were calculated from:

$$I = 1/2 \sum m_i z_i^2$$

where m and z are the molality and charge, respectively, acting on each dissolved ion. Data taken from Tables I and II indicate ionic strengths of 3.5

and 2.2 for the galena (200 C, ave.) and quartz (150 C, ave.) phases respectively. Precise calculation of the ionic strength for fluorite analyses was not possible, because calcium values were effected by the solubility of fluorite. Average values of 3.0 (at 200 C) and 2.0 (at 150 C) were adopted for further calculations.

Activity Coefficients

Activity coefficients of ionic species were calculated for each temperature of interest, using the ionic strengths of 3.0 and 2.0, and the averaged ion concentrations (Fig. IV). The Debeye-Huckel equation used for this is of the form:

$$\text{Log (Act.Coef.)} = \frac{Az(\text{exp})^2 I(\text{exp})^{1/2}}{1+aB*I(\text{exp})^{1/2} + B'I}$$

where A and B are the Debeye-Huckel parameters (Helgeson, 1967, p369), a is the effective radius of the ion in solution (Klotz, 1950), and B' is the deviation function (Helgeson, 1967, p751). Tabulated results are presented below:

Table VI

Activity Coefficients (Log)

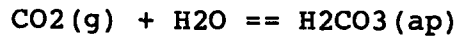
Ionic Species	Temperature	
	200 C	150 C
Pb	*	-3.0
Fe	-1.0	-.9
Zn	-5.0	-3.8
Ca	-1.02	-.88
Cl	-.36	-.30
F	-1.2	-.87
SO ₄	-1.47	-1.14
H ₂ S, H ₂ CO ₃	.24	.16

* - No data due to mineral solubility

fugacity of CO₂

The fugacity of CO₂ with respect to the analysed solutions can be calculated from the following relations:

$$\text{Log } H_2CO_3 = \text{log } m_{CO_2}(g) + \text{log } \Gamma(H_2CO_3)$$



where $m_{CO_2}(g)$ are the molal values determined from CO₂ pressures measured during extractions. Substitution of appropriate values for 150 and 200 C yields log f_{CO_2} values of 1.64 and 1.59 respectively.

pH

The Hansonburg deposit is characterized by open-space filling, with local replacement, of carbonate host. Thus equilibrium with calcite may be assumed for the mineralizing solutions. The pH of these solutions may then be calculated from:

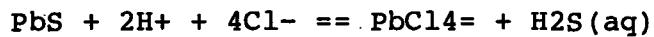


At 200 and 150 C the calculated pH of the depositional

fluids is 4.5, with neutral pH occurring at 5.64 and 5.82 respectively.

Activity of H₂S

From Helgeson's data (1969) one can calculate the most prevalent complex for the Pb-Cl species for high Cl solutions for these temperatures (150 and 200 C) as PbCl₄⁼. Using the analysed Pb values, and the ionization constant for PbCl₄⁼, one can compute the activity of H₂S from:



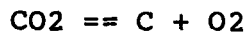
Assuming all Pb analysed was in the form PbCl₄⁼ while in solution, the lead data from the fluorite phase indicate a log H₂S of -7.46 (150 C, measured fluorite average). The calculation at 200 C (galena phase) is based upon an assumed concentration of 760 ppm Pb (fluorite data), and yields a log H₂S of -3.64.

fugacity of O₂, S₂

Ranges of values for f_{O2} and f_{S2} were obtained from graphical representation of equilibrium

calculations for the observed mineral species galena, sphalerite, pyrite, barite and anhydrite (Fig.16).

Minimum fO_2 limits were defined by:



assuming the presence of CO_2 during mineralization based upon the detection and measurement of CO_2 pressures during inclusion fluid extraction.

Maximum sulfate concentrations, relative to anhydrite presence during mineralization, were calculated using analysed Ca values and the relation:



This relation yielded values of $\log SO_4^{=}$ of -4.7 (150 C) and -5.56 (200 C).

The analysed values for Pb, Zn, Fe and Ca were used for the determination of their relative equilibrium lines. Maximum barium values were calculated from the maximum $SO_4^{=}$ calculations, above. This provides an approximation of the maximum barium concentrations to be expected in solution, relative to these two minerals (anhydrite and barite) presence at

the deposit. The results from Figure 16 indicate the following ranges:

150 C - $\log fO_2 = -43.0$ to -40.0

$\log fS_2 = -18.5$ to -16.0

200 C - $\log fO_2 = -40.0$ to -37.0

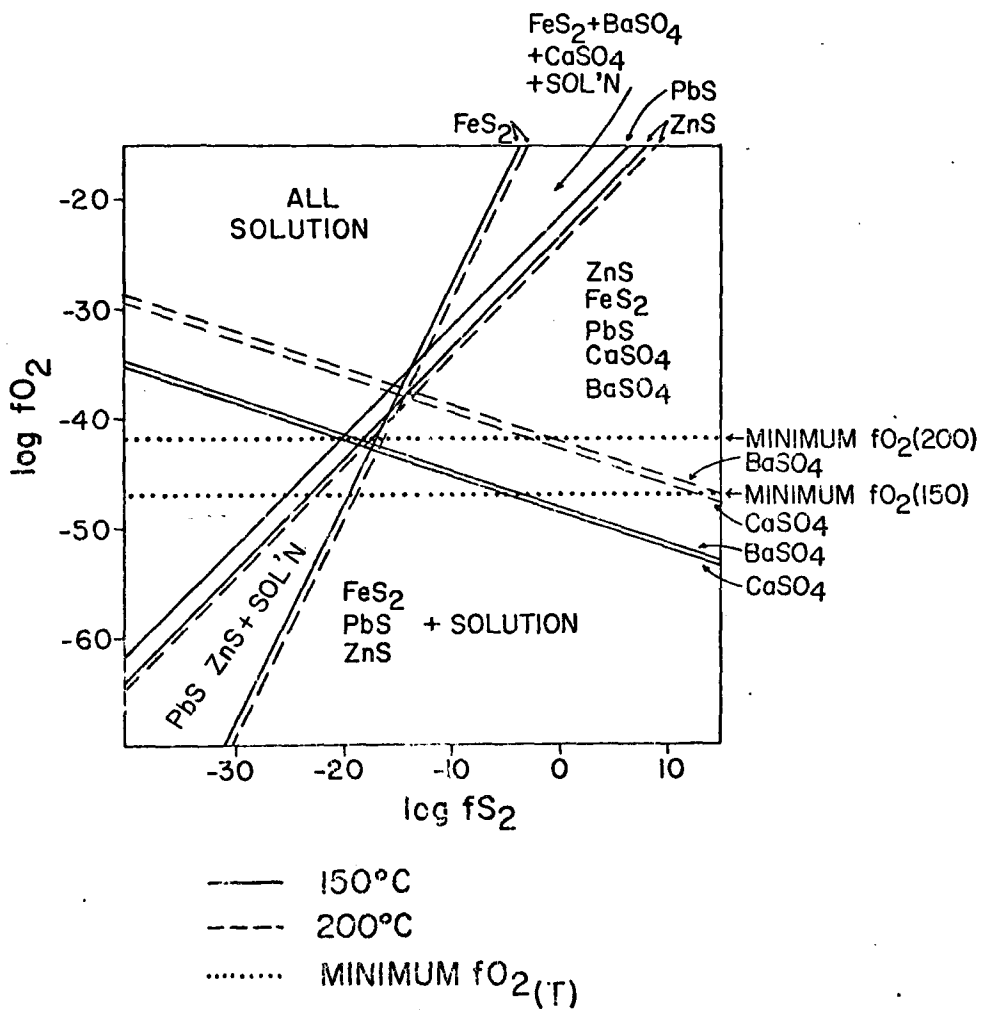
$\log fS_2 = -16.0$ to -13.5

Figure 16

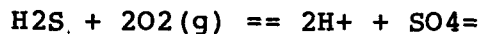
Equilibrium Equations	log K	
	150 C	200 C
Pyrite: $2\text{H}^+ + 1/2\text{O}_2 + \text{FeS}_2 == \text{Fe}^{++} + \text{S}_2 + \text{H}_2\text{O}$	10.73	9.86
Galena: $2\text{H}^+ + 1/2\text{O}_2 + \text{PbS} == \text{Pb}^{++} + 1/2\text{S}_2 + \text{H}_2\text{O}$	15.40	13.96
Sphalerite: $2\text{H}^+ + 1/2\text{O}_2 + \text{ZnS} == \text{Zn}^{++} + 1/2\text{S}_2 + \text{H}_2\text{O}$	16.32	14.24
Barite: $2\text{H}^+ + \text{BaSO}_4 == \text{Ba}^{++} + 1/2\text{S}_2 + 3/2\text{O}_2 + \text{H}_2\text{O}$	-65.7	-56.87
Anhydrite: $2\text{H}^+ + \text{CaSO}_4 == \text{Ca}^{++} + 1/2\text{S}_2 + 3/2\text{O}_2 + \text{H}_2\text{O}$	-65.7	-56.87
Carbon Dioxide: $\text{CO}_2 == \text{C} + \text{O}_2$	-48.74	-43.55

Figure based upon concentrations from Table IV; pH 4.5, log f_{CO_2} of 1.59 (200 C) and 1.64 (150 C) and log SO_4 of -5.56 (200 C) and -4.7 (150 C).

GRAPHICAL DETERMINATION OF RANGES FOR f_{O_2} AND f_{S_2} AT 150 AND 200°C



From an interpolation of Ohmoto's data (1972, p556) activity coefficients for SO_4^- ion in solution were determined (Table VI). Oxygen fugacity was calculated from:



At 200 and 150 C, the log f_{O_2} calculates at -39.03 and -42.95 respectively, indicating good agreement with the above ranges from the graphical representation.

Utilization of a similar relation, yields the value of fugacity of sulfur, for the above conditions:



which yields a f_{S_2} values of -11.25 and -17.18 (150 C), once again indicating good agreement with the graphical results.

Oxygen - sulfur fugacity diagrams were constructed at 150 and 200 C. The diagrams, (Figs. 17,18) indicate the stability fields for the various species, and show the region defined by the analyses of Hansonburg minerals.

Indicated by stippling are the f_{O_2} - f_{S_2} regions determined for the Hansonburg fluids (Figs. 16 and 17). At 200 C, Figure 16 indicates that the early

solutions were in equilibrium with galena, sphalerite, magnetite, hematite and pyrite. Later solutions (150 C, Fig. 17) indicate equilibrium with galena, sphalerite, hematite, anglesite and cerrusite. Pyrite and magnetite are no longer in equilibrium, while carbonates and sulfates have become stable.

Overall the calculations indicate a relative increasing oxygen fugacity as the temperature decreased. At 200 C, the f_{O_2} of the solution was in the magnetite-hematite-pyrite regions. At 150 C the calculated f_{O_2} is definitely above the magnetite field, and outside the pyrite field. Galena and sphalerite are stable at both temperatures, with equilibrium with anglesite and cerrusite (minor) being established at 150 C. From 200-150 C the f_{S_2} decreases slightly, shifting out of predominantly sulfide region, toward the sulfate field. The solutions appear to be buffered by the presence of hematite, magnetite, and pyrite.

Table VII

Tabulated Results - Thermodynamic Calculations

=====

Variable	Temperature	
	150 C	200 C
Ionic Strength	3.5	2.2
log fCO ₂	1.64	1.59
pH	4.5	4.5
log H ₂ S	-7.11	-3.64
log fO ₂ *	-42.95	-39.03
log fS ₂ *	-17.18	-11.25

=====

* - calculation based upon anhydrite presence

Figures 17 and 18

Equilibrium Equations	log K	
	150 C	200 C
Iron Species:		
$2\text{H}^+ + 1/2\text{O}_2 + \text{FeS}_2 == \text{Fe}^+ + \text{S}_2 + \text{H}_2\text{O}$	10.73	9.86
$2\text{H}^+ + 1/2\text{O}_2 + \text{FeS} == \text{Fe}^{++} + 1/2\text{S}_2 + \text{H}_2\text{O}$	21.00	18.34
$2\text{H}^+ + \text{FeCO}_3 == \text{Fe}^{++} + \text{CO}_2 + \text{H}_2\text{O}$	6.23	5.77
$4\text{H}^+ + \text{Fe}_2\text{O}_3 == \text{Fe}^{++} + 1/2\text{O}_2 + 2\text{H}_2\text{O}$	-13.20	-12.00
$6\text{H}^+ + \text{Fe}_3\text{O}_4 == 3\text{Fe}^{++} + 1/2\text{O}_2 + 3\text{H}_2\text{O}$	-8.76	-8.53
Lead Species:		
$2\text{H}^+ + \text{PbS} + 1/2\text{O}_2 == \text{Pb}^{++} + 1/2\text{S}_2 + \text{H}_2\text{O}$	15.40	13.69
$2\text{H}^+ + \text{PbSO}_4 == \text{Pb}^{++} + 1/2\text{S}_2 + 3/2\text{O}_2 + \text{H}_2\text{O}$	-67.61	-58.57
$2\text{H}^+ + \text{PbCO}_3 == \text{Pb}^{++} + \text{CO}_2 + \text{H}_2\text{O}$	5.55	5.52
Zinc Species:		
$2\text{H}^+ + \text{ZnS} + 1/2\text{O}_2 == \text{Zn}^{++} + 1/2\text{S}_2 + \text{H}_2\text{O}$	16.32	14.24
$2\text{H}^+ + \text{ZnCO}_3 == \text{Zn}^{++} + \text{CO}_2 + \text{H}_2\text{O}$	7.32	6.92

Figure 17. Stability fields for indicated mineral phases at $f\text{CO}_2 = 38.90$ and $T = 200$ C. Stippled region is defined by analysis of Hansonburg fluids. Diamond indicates PATH results for Hansonburg fluids.

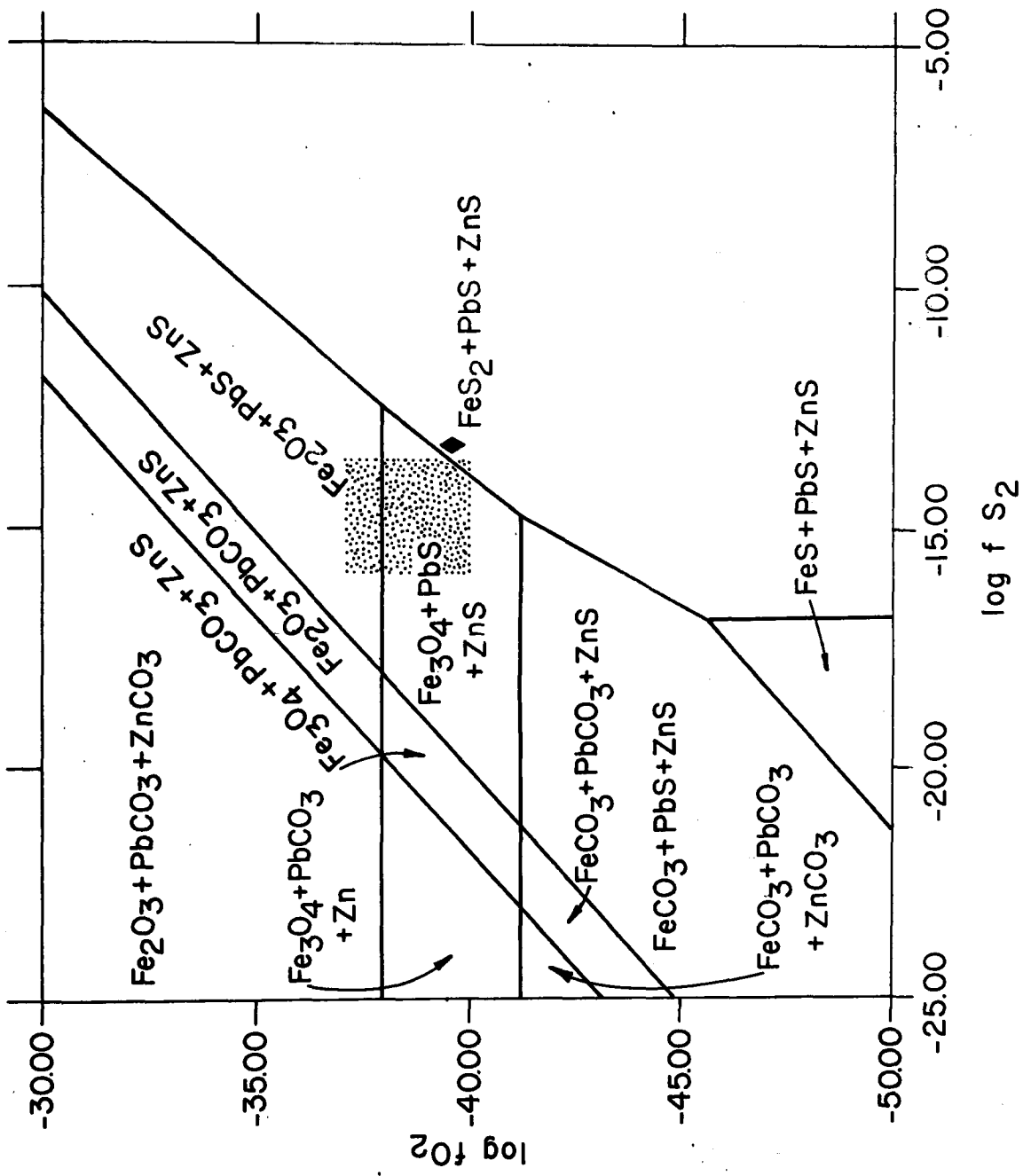
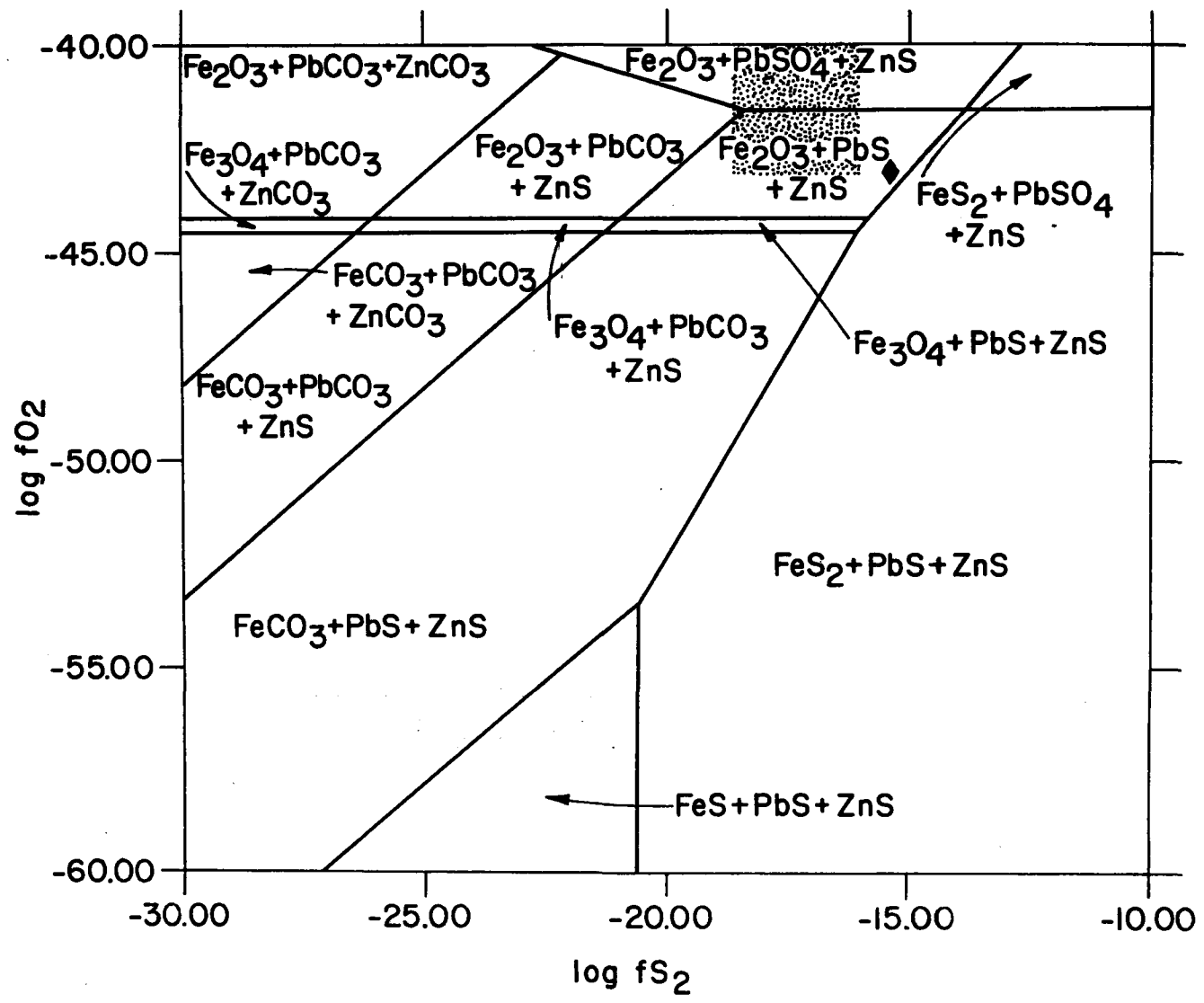


Figure 18. Stability fields for indicated mineral phases at $f_{CO_2} = 43.65$ and $T = 150$ C. Stipled region is defined by analysis of Hansonburg fluids. Diamond indicates PATH results for Hansonburg fluids.



Fugacity of O_2 - pH diagrams were constructed to determine the prevalent sulfur species at 200 and 150 C (Fig. 19). The diagrams indicate a shift out of the H_2S field, into the sulfate field from 200 to 150 C (Fig. 19). This indicates that later solutions (150 C) favor the formation of sulfate minerals rather than sulfide. This agrees well with the notable lack of any "low-temperature" sulfide minerals at the Hansonburg deposit, while massive barite predominates.

Similarly, this reinforces the region shift depicted in Figures 17 to 18, and again supports the (Na/K) calculated temperatures for the galena phase, as this phase would only be stable at the higher temperatures. PATH indicates a similar, though smaller shift in the predicted sulfur species.

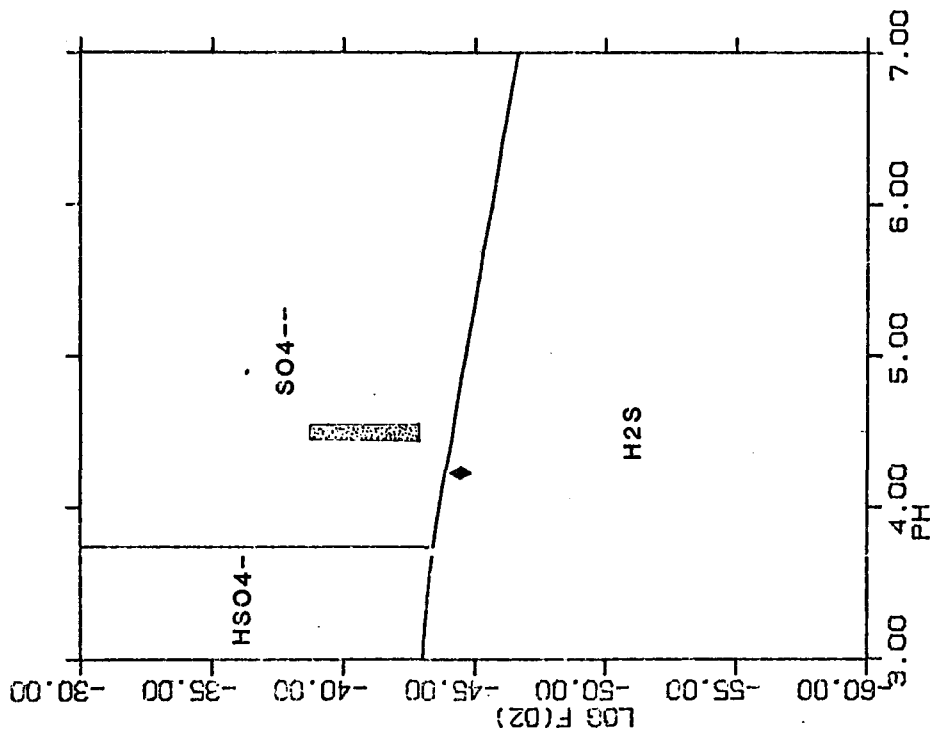
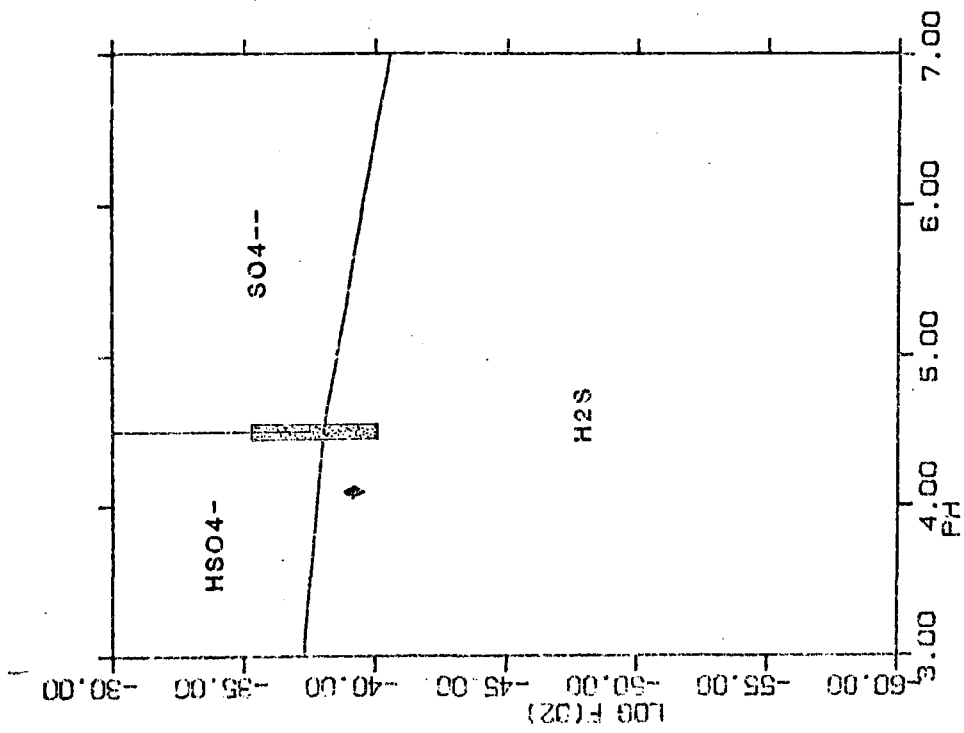
Figure 19

Log fO₂ vs pH plot for Sulfur Species

Equilibrium Equations	log K	
	150 C	200 C
Sulfur Species		
SO ₄ ⁼ == SO ₄ ⁼	0.0	0.0
HSO ₄ ⁻ == H ⁺ + SO ₄ ⁼	-3.74	-4.49
H ₂ S + 2O ₂ == SO ₄ ⁼ + 2H ⁺	79.31	67.13
H ₂ S + 2O ₂ == H ⁺ + HSO ₄ ⁻	83.05	71.62

(Helgeson, 1969)

Figure 19. Stability fields for sulfur species H₂S, HSO₄⁻ and SO₄⁼ at 200 C (left) and 150 C (right). Stipled region is defined by analysis of Hansonburg fluids. Diamond indicates PATH results for Hansonburg fluids.



PATH Calculations

A version of the PATH program used at N.M.I.M.T. was applied to the analytical data. Reactant minerals were specified as calcite and pyrite, as in the previous calculations. Concentration data were entered directly into the program, with the exception of chloride values. Chloride values proved to be insufficient for PATH, and had to be adjusted to permit computation. Slight differences from this authors results will be noted, which are due to: 1. The use of different equilibrium constants than those used by this author and, 2. the capability of the program to evaluate all species virtually at once, something which is not possible in hand-calculated equilibriums.

Results of PATH calculations (Table VIII) show excellent agreement with both the graphical determination and the hand-calculated results. PATH calculations precipitate large amounts of siderite toward the end of the data reduction, with three-orders of magnitude greater amounts in the 150 C calculation than in the 200 C calculation. This supports this authors designation of siderite as representing later stages of mineralization.

Table VIII

Tabulated Results - PATH Computer Program

```
=====
```

PATH Results	Temperature	
	150 C	200 C
Ionic strengths	3.2	2.5
log fCO2	1.72	1.73
pH	4.37	4.14
log H2S	-5.54	-4.53
log fO2	-44.22	-39.42
log fS2	-15.31	-13.43
log H2S *	-5.74	-4.87
log fO2 *	-43.43	-38.05
log fS2 *	-14.92	-12.74

```
=====
```

* - PATH calculations based upon anhydrite presence

Chemical Model

The above thermodynamic calculations indicate that the observed mineralization is not resultant from any drastic changes in solution chemistry, rather it is resultant from primarily a drop in temperature.

Early, hot solutions entered the limestone units, reacted only minorly with the calcite, and precipitated early sulfides (PbS, ZnS, FeS₂) and then massive fluorite. Sulfate (Pb, Ba, Ca-SO₄) deposition is indicated for both early and late solutions, though it is the only sulfur species stable in the cooler (150 C) solutions. This supports mineralization observations made in the field.

The siderite stability field is not entered by the solution regions, although it represents a significant phase in the district. This suggests that the siderite depositing solutions were different from those analysed during this study, and supports this author's previous assertions.

Depth of Mineralization

Calculations of minimum confining pressures during mineralization based upon the average salinity of 15 eq.wt.% NaCl from inclusion measurements, indicate pressures on the order of 115 bars, assuming Roedder's

(et al., 1968) 1500 meters of depth (Haas, 1971). This would certainly seem to be the maximum, considering that the open-space within the limestone was most likely connected with the surface during mineralization.

CO₂ pressures, paired with minimum H₂O pressures to be expected during mineralization, enable an estimate of the minimum confining pressure (hydrostatic) during mineralization. At 200 C, H₂O boils at less than 16 bars pressure. For this temperature (and pressure) regime the activity coefficient for CO₂ is roughly equal to unity, therefore the f_{CO_2} equals CO₂ pressure. Thus, the f_{CO_2} of 53.70 (200 C), plus the minimum H₂O pressure of 16 bars (no boiling indicated for Hansonburg fluids), indicate pressures on the order of 70 bars during the mineralization. This pressure corresponds to approximately 700 meters of depth (and 290 C) for solutions of 15 eq.wt.% NaCl (Haas, 1971).

SOURCE OF MINERALIZING SOLUTIONS

Analyses from numerous wells in the gulf coast area, southern Louisiana (Randolph et al., 1980) (Table VII), indicate remarkable similarities to the analyses from the Hansonburg district. These 90-130 C formational waters are characterized by Na-Cl brines. The values of Na and Cl are not significantly different from those values detected in this study. Calcium values are well within the range defined by the quartz analyses. The only significant differences are the Mg, K and various metal values (not shown). Magnesium is noticeably higher in the formational waters, indicating, perhaps the presence of dolomite in the containing sediments. Potassium values are quite a bit lower, though the significance of this is not certain. Metal values are not reported from all wells, though where reported are 0-60 ppm, significantly lower than those values detected in this study.

Hall and Friedman (1963) noted similar agreement between their fluid inclusion analyses and present day oil field-brines from the host St. Genevieve Limestone. Averaged concentrations and ion-ratios from their analyses are not significantly different from the concentrations reported from present-day connate waters

in southern Illinois.

The Louisanna formation-well samples, taken at great depth and temperature, cooled and depressurized rapidly upon reaching the surface. This resulted in the precipitation of solid phases within the sampling container. The phases detected by X-ray diffraction are galena, sphalerite, barite, quartz, calcite and halite. Unidentified fine-grained precipitates show the presence of major amounts of Fe, Ca, Ba, Cl and locally Zn, with minor and trace constituents of Sr, Si, Cu, Ni, K, Br and S (by X-ray fluorescence).

The presence of these solid phases paired with the analyses of the formational waters (Table VII) indicate rather remarkable similarities between the formation waters and the fluids responsible for the Hansonburg mineralization. As indicate above, these solid phases precipitated out of the formation-waters upon a decrease in pressure and temperature.

Randolf et al. (1980) and Bebout (1980) indicate measured temperatures of the formation waters from 201-267 F (94-131 C). The general temperature gradient for south Louisiana, in the geopressured zones which contain these fluids creates 100 C at -3,350 meters depth, and 150 C near -4,880 meters. Local variations are detected near fault zones and are believed to be resultant from the migration of the geopressured fluids

into the faults ("hydropressure zone") (Bebout, 1980). The pressures detected in these geopressurized zones is on the order of 830 bars.

The present author proposes therefore, that the fluids responsible for the formation of the Hansonburg deposit were derived from within the sedimentary pile presently containing the deposits. Although the depth of sedimentary cover at the time of ore formation was not as deep as that found in the present day Louisiana area, high temperatures in accord with those observed in the Louisiana region would be created, in considerably less sedimentary thickness, by the location of these Hansonburg sediments within an active rifting environment, with its greatly elevated regional heat-flow.

Of considerable interest is the continued Sr values indicated by Randolph et al. (1980). The values (not shown) range from 340-1,300 ppm, and averaged 760 ppm. Strontium was not analysed in this study, though Kopicki (1963) noted its unusual distribution throughout the district. Kopicki reports that the limestones in the area, while not containing significant Sr concentrations, contain anomalous ubiquitously high concentrations on faults that may have played a role in mineralization.

Lead isotope studies indicate, as in other Mississippi Valley-type deposits, that the Hansonburg leads are highly radiogenic, J-type leads (Austin and Slawson, 1961; Ewing, 1979; and others). Their data suggest a crustal source for the leads, calling on leaching of a Precambrian terrain. Beane (1974) proposed a model with deep convection of near-surface waters into the Precambrian basement, in a model similar to that proposed for the Mississippi Valley deposits by Heyl et al. (1974).

Permian arkoses overlying the Hansonburg deposit, however, contain detrital sediments (feldspar) derived from Precambrian basement rocks (the Pedernal uplift in Pennsylvania time) and could also supply the radiogenic leads (Allmendinger, 1975).

The presence of high fluorine concentrations together with the differences between the metal values detected at the Hansonburg deposit and the values reported from the Louisiana formational waters, with the lead isotope interpretations, suggests a different source for the metals and the fluorine. However, concentrations reported from the oil field brines in Central Mississippi indicate metal values (Pb, Zn, Fe) quite similar to those detected in this study (Carpenter et al., 1974). The values (not shown) indicate that formational waters are quite capable of

attaining the concentrations necessary for metal-sulfide deposition, without any other fluid source (ie. - magmatic). These solutions precipitate barite and galena when brought to the surface, as did the formation waters in Louisiana.

The world-wide association of fluorine with rifting environments is well-documented (C.E.Chapin, 1980, pers. commun.). Perhaps the inclusion waters found in this study are fluoride-enriched formational waters which derived high fluorine concentrations from their containment within a rift-related basin.

The "state-wide" association of ore deposits of the Hansonburg assemblage with the margins of the Rio Grande rift (Fig. 20), has been well noted (Allmandinger, 1975; Beane, 1974; and others). The majority of the numerous deposits along the margins of the Rio Grande rift occur as vein and fracture filling, occupying available open-space in a variety of rock types. The Hansonburg deposit is merely a more extensive development of the same type, and sequence of mineralization. This suggests that the solutions responsible for the Hansonburg deposit were no different than those solutions responsible for the numerous other deposits along the rift, but that the rock hosting the Hansonburg deposits contained greater amounts of karst-related open-space. Beane (1974)

reports that fluid inclusion and stable isotope data from a number of the deposits suggest a "common genetic link" among the deposits. This author proposes that the "common genetic link" referred to by Beane (1974) is the presence of these formational waters over a large region which then ascended along rift-related structures, and deposited the observed mineralization (Fig. 20).

Early phase, terminated quartz crystals observed in this study, exhibited highly variable initial growth temperatures, and, as quartz precipitation is primarily in response to a drop in temperature, (while changes in pH, fO₂, etc., do not so greatly effect silica solubility) may represent the entrance of the hot, mineralizing solutions into the slightly cooler host rock. Formational waters temperatures are found to increase toward the center of large basins, and decrease out toward the margins. These waters are driven to the margins of the basin by compaction, which is greatest in the center of the basin. Thus the margins of the basins related to the Rio Grande rift would be favorable sites for migration, and ultimately ascension of the waters by the utilization of rift-related fractures. The location of the Hansonburg deposit (and all the other deposits - Fig. 20) would be similarly favorable sites.

Figure 20

Locations of galena, barite and fluorite occurrences relative to the margins of the Rio Grande rift in New Mexico (after Beane, 1974).

limestone (the fossil is within the upper part of space)
which are lithologically more fossiliferous than the

part
the
thou
is
line
of t
Spr
Bur
niet

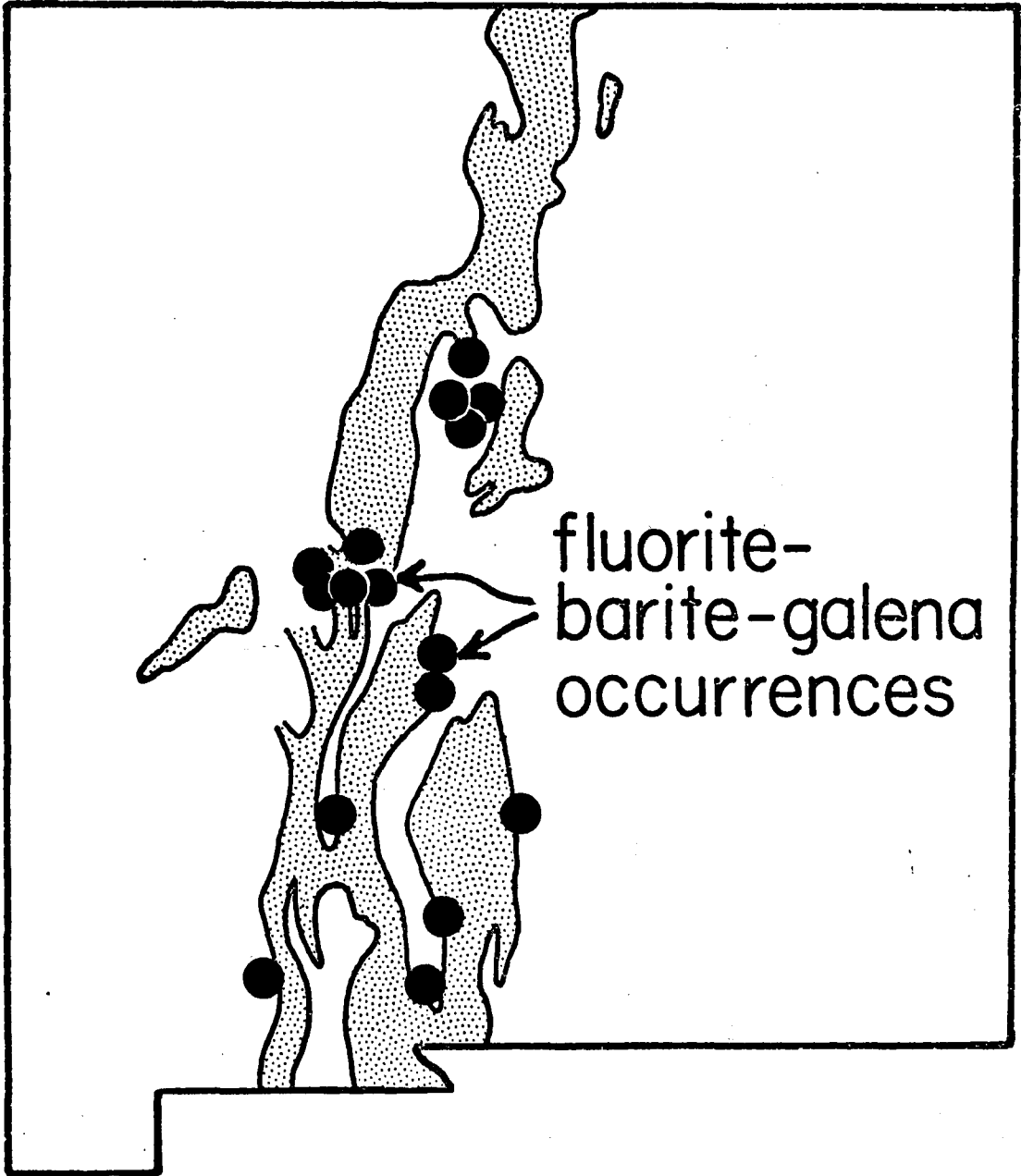


spot-holed (perhaps a fossiliferous limestone)

con
xat
depo
Tyn
con
Cen
min
type



throughout the central part of the section
been related to the region of the



fluorite-
barite-galena
occurrences

GENETIC MODEL

Ground Preparation

Early crustal structures (Precambrian), such as the Capitan lineament, were quite active from Cambrian through, at least, Paleozoic time. Characteristic pinching out of certain strata (Cambrian - Pennsylvanian and younger) adjacent to, and sub-parallel to lineaments indicate some relative differential uplift across the lineaments. These structural and topographic highs are likely environments for the formation of the observed reef-facies limestone characteristic of the Hansonburg district. Disconformities within the sediments overlying this favorable host indicate both a depositional hiatus, and erosional surface. Karstification of the porous reef-facies accompanied this uplift, resultant in numerous caves and sink hole features.

Rio Grande Rift

Continental rifting, in early formational stages, would create a vast basin, filled with an extensive sedimentary pile. Formation waters, characteristic of

deep sedimentary basins, would show elevated temperatures due to the anomalously high heat-flow associated with the rift. The waters would exhibit isotopic fractionations and solution chemistry reflective of the containing sedimentary pile. Early rift-opening tectonics would create differential lateral displacement along the intersection of the Capitan lineament with the rift, resulting in high-angle normal faults "fanning" from one structure's orientation to the other's. These faults would intersect the formation waters at depth, providing access ways toward the surface, into the overlying sediments.

Mineralization

These heated formational waters migrating out of the center of the sedimentary basin, ascending up and along fractures, in response to a decrease in confining pressure, would readily move laterally in the more porous strata of the karstified units. Entrance of these solutions into slightly cooler rock results in initial mineralization (quartz) that is confined to the wall-rock solution interface due to the temperature difference between the two. Minute solid phases precipitating from the cooling solutions would be

carried along by the fluids, settle out and be trapped in early phase minerals. This would explain the observation of fluorite mineralization being confined to the floor of certain caverns not completely filled with mineralization. Thus mineral precipitation is primarily in response to a drop in temperature and pressure, and is not dependent upon either host lithology or solution-rock reaction.

DISCUSSION OF SIMILARITIES BETWEEN THE
HANSONBURG DISTRICT AND THE CAVE-IN-ROCK DEPOSITS
OF SOUTHERN ILLINOIS

Stratigraphy

Both deposits are hosted in Paleozoic sediments (predominantly Pennsylvanian Aged) which directly and unconformably overly the Precambrian crystalline basement.

The presence of depositional hiati on top of each of the banded-host imply the potential for pre-mineralization development of karst. This would explain: 1. The predominance of open-space filling exhibited in the ores. 2. Sharp transitions from barren to mineralized host. 3. The presence of similar mineralized cavities adjacent to cavities void of mineralization.

Continental Rifts

The proximity of the Rio Grande rift and the Hansonburg deposits has been stated above. The presence of a mid-continental rift (aulocogen) in the Mississippi embayment has been proposed for a number of years. The New Madrid fault zone is thought by some to represent the present day expression of this presumably

Proterozoic feature. Recent geophysical work of Hildenbrand and Kucks (1980) delineate a rather pronounced magnetic profile based upon second vertical derivatives of the total magnetic field intensity. They define the structure, which is "completely masked by thick sedimentary strata" as being a graben that developed in the Precambrian surface, during a stage of pre-Late Cambrian rifting (Hildenbrand and Kucks, 1980). Their structure shows a notable loss of definition in the region of the Cave-in-Rock district, along an east-west trend which seems to correlate with the zone marking the intersection of the proposed 38th Parallel lineament.

Lineaments

The presence of a west-trending lineament (the 38th Parallel Lineament) in the Cave-in-Rock area has been proposed by Heyl (1972). He documents the regional feature by criteria similar to those described by Chapin et al. (1978) and others: 1. The alignment of structures (right-lateral wrench faults) that cross the Blue Ridge Mountains. 2. Subtle bends and terminations in several Appalachian folds where they intersect the lineament. 3. A 70 mile long westward-extended swarm of Mesozoic intrusives. 4.

Stratigraphic changes (which intensify westward) across the lineament, from Precambrian through and including the Mississippi and lower Pennsylvanian sediments. 5. Right-lateral offset of the axis of the Cincinnati arch. 6. Separation of the Illinois Basin to the north, from the Kentucky coal fields to the south.

Recently, Swadley (1980) described the pinching-out of certain Ordovician strata of the Drakes Formation just east of Louisville, Kentucky. He defines the units as being an off-shore tidal complex of Upper Ordovician Age. The present author feels, due to the location of these facies and the orientation of their respective northern and southern limits, that they may be resultant from the differential uplift across the lineament (Chapin, 1979). The occurrence of reef-facies in such an environment, as stated earlier, is highly likely.

Local Structure

The presence of structural features or lineaments, and the presence of (or indicated presence of) a mid-continental rift result in quite similar regional structures. As defined by Chapin (1979), these areas of intersections of structures with lineaments create structurally complex areas. A comparison of figures 4, 5 and 21 show the predominant structures resultant

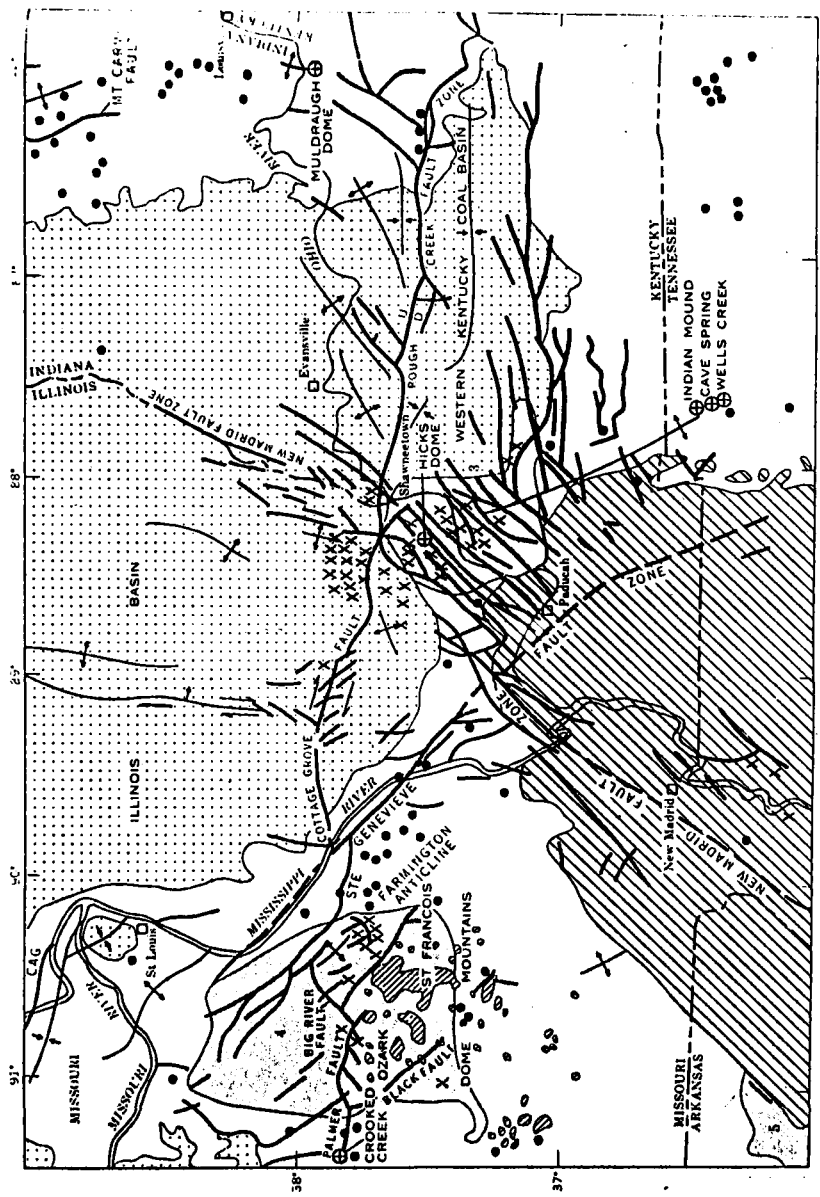
from these intersections. As noted in the Hansonburg area, the southeast trending faults which localized the mineralization fan from the westward trend of the Capitan lineament (Jones Camp dike) to the north-south trend of the Rio Grande rift. A similar feature is shown in Figure 21, which exhibits the "fanning" of the normal faults of the Cave-in-Rock district from a westward trend (of the 38th Parallel lineament) to the southwest trend of the New Madrid fault zone. These areas of fanning structures represent the response of the involved strata to the stresses imposed by the intersections of two structural trends.

Of prime interest here is the location of these two distinct districts. Both are located at the intersection of a lineament and a rift. Ages of the activity along these rift structures is not of too great a concern, for both show some indication of recurrent activity, though the Rio Grande rift is certainly more active. Both lineaments show evidence of some component of lateral movement. Heyl (1972) indicates right-lateral movement across the 38th Parallel lineament, while the present author visualizes a slight component of left-lateral movement across the Capitan lineament (with C.E. Chapin, 1980, oral commun.). The abrupt termination of the east-bounding fault of the Rio Grande rift immediately north of the



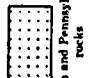
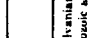

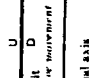
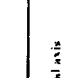

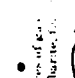
Hansonburg district marks the intersection of that boundary and the Capitan lineament. Similarly, the seemingly abrupt termination of the Mississippi Embayment-graben (Hildenbrand and Kucks, 1980, Cover Figure) may mark its intersection with the 38th Parallel lineament.

Figure 21

Map of the Cave-in-Rock deposits (3) of Southern Illinois, showing regional structures and location of 38th Parallel lineament (after Heyl, 1972).



EXPLANATION

	Tertiary and Cretaceous rocks		X
	Permian and Pennsylvanian rocks		
	Pre-Mississippian rocks		
	Anticlinal axis		
	Cryptosplaxion structure		

Occurrences of gas-splalherite, barite, etc.

Large mineral dist.

1. Illinois-Kentucky
2. Southeast Miss.
3. Northeast Ark.

Scale: 0 25 50 100 MILES

Ore Horizon

The "favorable horizon" in both districts is an allochthonous, reef-facies limestone which favors karst development. The Ste. Genevieve limestone in the Cave-in-Rock district is characterized by the alternation of limestone beds of varying purity, similar to the Council Springs Unit in the Hansonburg district. Karstification of this unit results in horizontal caves which are occupied by later mineralization (the "perfectly banded ore" of Grogan and Bradbury, 1967). The formation of this reef-facies is postulated as being resultant from differential uplift across the 38th Parallel lineament during sedimentation.

Both districts are established upon the more extensive mineralization developed within the banded-limestone host. Though other occurrences, such as veins and fissure fillings are present within and peripheral to these districts, the most extensive mineralization is present in the banded-rock. The fact that a similar mineral assemblage occurs in a wide range of rock types, indicates that the solutions did not need to react with a carbonate host to deposit the observed phases, but merely need pre-existing open-space through which the solutions migrated.

Mineralogy

The ores from both districts exhibit a banded or "coontail" layering reflective of the paragenetic sequence of the mineralization. Both deposits are characterized by the predominance of fluorite and galena, though Cave-in-Rock possesses more sphalerite, and the Hansonburg more barite and quartz. All involved mineral species are present within both districts.

Fluid Inclusions

Freas (1961) reports homogenization temperatures from 90-140 C, as compared to the Hansonburg inclusions which homogenized from 130-210 C. Hall and Friedman's analysis of the Cave-in-Rock inclusion fluids yield concentration data which are not significantly different from the values detected in this study of the Hansonburg deposits. Other than possessing slightly higher filling temperatures, the Hansonburg inclusions are remarkably similar to those found at Cave-in-Rock in deposits in Southern Illinois.

SUMMARY AND CONCLUSIONS

Field observations of the Hansonburg mineralization indicate ore characteristics which relate to pre-existing sedimentary structures within a reef-facies limestone. These sedimentary structures seem to be resultant from differential uplift along lineaments during deposition of the limestone. Pre-mineralization development of karst solution-ways within these sedimentary structures created the open-space utilized by the mineralizing fluids.

Fluid inclusion homogenization temperatures indicate fluid temperatures in the range 130-210 C, characterized by Na-Cl brines. Variations in the observed general paragenetic sequence, paired with anomalously high homogenization temperatures, suggest the activity of nearby faults in the mineralizing process.

Analyses of inclusion fluids yields data which are remarkably similar to other Mississippi Valley-type deposits, and to present day formational waters. Thermodynamic calculations based upon the analyses indicate that the solutions did not change much during the course of mineral deposition. The calculations predict both the mineralization and paragenetic sequence observed in the district. Solution-wall rock

interaction does not seem to be important, rather, mineralization appears to be resultant from primarily a decrease in temperature (and pressure) of nearly saturated solutions.

The numerous remarkable similarities between the Hansonburg deposits and the Cave-in-Rock deposits of Southern Illinois are less than coincidental. A geologic history and genetic model similar to that proposed for the Hansonburg is here proposed for the two districts.

REFERENCES

- Allmandinger, R.J. (1974) Source of ore forming fluids at the Hansonburg mining district, central New Mexico (abs): Geologic Society of Amer., v.6, n.7, p633
- Allmandinger, R.J. (1975) A model for ore-genesis in the Hansonburg mining district, New Mexico: unpublished M.S. thesis, New Mexico Institute of Mining and Technology, 190p.
- Ames, L.L., Jr. (1958) Chemical analysis of the fluid inclusions in a group of New Mexico minerals: Econ. Geol., v.53, p.473-480.
- Anderson, G.M. (1975) Precipitation of Mississippi Valley type ores: Econ. Geol. v. 70, p937-942.
- Austin, C.F. and Slawson, W.F. (1961) Isotopic analysis of single lead crystals: A clue to history of deposition: Amer. Mineral. v. 46, p1132-1140.
- Beales, F.W. (1975) Precipitation mechanisms for Mississippi Valley-type ore deposits: Econ. Geol. v. 70, p943-948.
- (1976) (reply to discussion by Ohle, 1976): Econ. Geol. v. 71, p1062-1064.
- Beales, F.W. and Jackson, S.A. (1966) Precipitation of lead-zinc ores in carbonate reservoirs as illustrated by Pine Point ore field, Canada: Inst. Mining Metallurgy Trans., sec. B, v. 75, p278-285.
- Beane, Richard E. (1974) Barite-fluorite-galena deposits in south- south-central New Mexico: A product of shallow intrusions, groundwater, and epicontinental sediments (abs): Geol. Soc. Am., Abstracts with programs, v.6, n.7, p.646-647.
- Bebout, D.G. (1980) Physical properties of reservoir fluids, Quarterly report: The Energy Programs Office, Louisiana State Univ., (Draft).
- Brown, J.S. (Editor), (1967) Genesis of stratiform lead-zinc-barite-fluorite deposits (Mississippi Valley type deposits), a symposium: The Economic Geology Publishing Co. Monograph 3, 443p.

- Carpenter, A.B., Trout, M.L. and Pickett, E.E. (1974) Preliminary report on the origin and chemical evolution of lead-and zinc-rich oil field brines in Central Mississippi: *Econ. Geol.*, v. 69, pl191-1206.
- Chapin, C.E. (1979) Evolution of the Rio Grande Rift - A summary, in Rieker, R.E. ed., *Rio Grande Rift: Tectonics and Magmatism*: Washington, D.C., Amer. Geophy. Union, pl-5.
- Chapin, C.E., Chamberlin, R.M., Osburn, G.R., Sanford, A.R., and White, D.W. (1978) Exploration Framework for the Socorro geothermal area, New Mexico, in Chapin, C.E., and Elston, W.E., eds., *Field guide to selected cauldrons and mining districts of the Datil-Mogollon volcanic field, New Mexico*: New Mexico Geological Society, Spec. Pub. No. 7, pl15-130.
- Chapin, C.E., Osburn, G.R., Hook, S.C., Massingill, G.L., and Frost, S.J. (1979) Coal, Uranium, Oil and Gas Potential in the Riley-Puertecito Area, Socorro County, New Mexico: New Mexico Energy Institute, New Mexico Institute of Mining and Technology, Socorro, New Mexico, 33pp.
- Doe, B.R., Hedge, C.E. and White, D.E. (1966) Preliminary investigation of the source of lead and strontium in deep geothermal brines underlying the Salton Sea geothermal area: *Econ. Geol.* v. 61, p462-483.
- Doe, B.R. and Delevaux, M.H. (1972) Source of leads in Southeast Missouri galena ores: *Econ. Geol.* v. 67, p409-425.
- Eardley, A.J. (1962) *Structural Geology of North America*: New York, Harper and Row, 743pp.
- Ewing, T.E. (1979) Lead isotope data from mineral deposits of southern New Mexico: A reinterpretation: *Econ. Geol.*, v.74, p.678-684.
- Garrels, R.M. and Christ, C.L. (1965) *Solutions, Minerals, and Equilibria*, New York, Harper and Row, 450p.
- Garrels, R.M. and Dreyer, R.N. (1952) Mechanisms of limestone replacement at low temperatures and pressures: *Geol. Soc. Amer.*, v. 63, p325-380.

- Gerdemann, P.E. and Myers, H.E. (1972) Relationships of carbonate facies to ore distribution and to ore genesis in the Southeast Missouri Lead district: *Econ. Geol.*, v. 67, p426-433.
- Grogan, R.M. and Bradbury, J.C. (1968) Fluorite-zinc-lead deposits of the Illinois-Kentucky Mining District, in Ridge, J.D. ed., *Ore Deposits of the United States, The Graton Sales Volume: New York, American Inst. of Mining, Metallurgical, and Petroleum Engineers, Inc.*, p.370-399.
- Haas, Jr, J.L. (1971) The effect of salinity on the maximum thermal gradient of a hydrothermal system at hydrostatic pressure: *Econ. Geol.*, v.66, p940-946.
- Hall, W.E. and Friedman, Irving (1963) Composition of fluid inclusions, Cave-in-Rock fluorite district, Illinois, and Upper Mississippi Valley lead-zinc district: *Econ. Geol.*, v.58, p.886-911.
- Head, R.E. (1932) The cleavage surfaces of galena: *Amer. Mineral.*, v.16, no.9, p345-31.
- Helgeson, Harold C. (1966) Solution chemistry and metamorphism, in Abelson, P.H., ed., *Researches in Geochemistry*, v.II: New York, Wiley and Sons, p.362-404.
- (1969) Thermodynamics of hydrothermal systems at elevated temperatures and pressures: *Am. Jour. Sci.*, v.267, p.729-804.
- (1970) A chemical and thermodynamic model of ore deposition in hydrothermal systems, in Morgan, B.A., ed., *Fiftieth Ann. Symposia: Min. Soc. Am.*, Spec. Paper 3, p.133-186.
- Helgeson, H.C., Brown, T.H., and Leeper, R.H. (1969) *Handbook of Theoretical Activity Diagrams Depicting Chemical Equilibria in Geologic Systems Involving an Aqueous Phase at One Atmosphere and 0 to 300 C.*, San Francisco, Freeman, Cooper and Co., 253p.
- Helgeson, H.C., Brown T.H., Nigrini, A., and Jones, T.A. (1970) Calculation of mass transfer in geochemical processes involving aqueous solutions: *Geoch. et Cosmoch. Acta*, v.34, p569-592.

- Heyl, A.V. (1972) The 38th Parallel lineament and its relation to ore deposits: *Econ. Geol.*, v. 67, p879-894.
- Heyl, A.V., Delevaux, M.H., Zartman, R.E. and Brock, M.R. (1966) Isotopic study of galenas from the Upper Mississippi Valley, the Illinois-Kentucky, and some Appalachian Valley mineral districts: *Econ. Geol.*, v. 61, p933-961.
- Heyl, A.V., Landis, G.P. and Zartman, R.E. (1974) Isotopic evidence for the origin of Mississippi Valley-type mineral deposits: a review: *Econ. Geol.*, v. 69, p992-1006.
- Hildenbrand, G. and Kucks, R.P. (1980) (cover illustration and caption): *EOS*, v. 61, p577.
- Holland, H.D. and Malinin, S.D. (1979) The solubility and occurrence of non-ore minerals, in Barnes, H.L. ed., *Geochemistry of Hydrothermal Ore Deposits*: 2nd edition, New York, Wiley and Sons, p461-508.
- Kelley, V.C. and Thompson, T.B. (1964) Tectonics and General Geology of the Ruidoso-Carrizozo Region, Central New Mexico, in *Ruidoso Country: New Mexico Geological Society Guidebook 15*, p110-121.
- Klotz, I.M. (1950) *Chemical Thermodynamics*: Englewood Cliffs, N.J., Prentice Hall, p. Fluid inclusions in quartz from deep-seated granitic intrusions, south Norway: *Lithos*, v. 12, p13-23.
- Kopicki, Robert J. (1962) Geology and ore deposits of the Northern part of the Hansonburg mining district, Bingham, New Mexico: unpublished M.S. Thesis, New Mex. Inst. of Min. and Tech.
- Kottlowski, Frank E. (1953) Geology and ore deposits of a part of the Hansonburg mining district, Socorro County, New Mexico: *New Mex. Bur. of Mines and Min. Res., Circ. 23*, 9 p.
- (1960) Summary of Pennsylvanian Sections in Southwestern New Mexico and Southeastern Arizona: *New Mexico Bur. Mines Min. Res., Bul. 66*, 187pp.
- Lasky, S.G. (1932) The ore deposits of Socorro County, New Mexico: *New Mex. Bur. of Mines and Min. Res., Bulletin 8*.

- Lewchalermvong, C. (1973) Investigation and evaluation of the Royal Flush and Mex-Tex mines, and adjacent area, Hansonburg Mining District, Socorro County, New Mexico: unpublished M.S. Thesis, New Mex. Inst. of Min. and Tech.
- Norman, D.I. (1977) Geology and geochemistry of Tribag mine, Batchawana Bay, Ontario: unpublished Ph.D. Thesis, University of Minnesota-Duluth.
- Ohle, E.L. (1959) Some considerations in determining the origin of ore deposits of the Mississippi Valley type: Econ. Geol. v. 54, p769-789.
- (1976) Discussion of paper by Beales, 1975: Econ. Geol. v. 71, p1060-1061.
- (1980) Some considerations in determining the origin of ore deposits of the Mississippi Valley type, Part II: Econ. Geol., v.75 p.161-172.
- Ohmoto, Hiroshi (1972) Systematics of sulfur and carbon isotopes in hydrothermal ore deposits, Econ. Geol., v.65, p.551-578.
- Randolph, P.L., Rockar, E.M. and Osif, T.L. (1980) Gas saturation in formation waters, Annual report for 1979: Inst. of Gas Tech., Illinois Inst. Tech., Chicago.
- Richardson, C.K. and Holland, H.D. (1979) The solubility of fluorite in hydrothermal solutions, an experimental study: Geochem. Cosmochem., v. 43, p1313-1325.
- (1979) Fluorite deposition in hydrothermal systems: Geochem. Cosmochem., v.43, p1327-1335.
- Roedder, E. (1958) Technique for the extraction and partial chemical analysis of filled fluid inclusions from minerals, Econ. Geol., v.53, p.235-269.
- (1962) Studies of fluid inclusion I: Low temperatures application of a dual-purpose freezing and heating stage: Econ. Geol., v.57, p.1045-1061.
- (1963) Studies of fluid inclusion II: Freezing data and their interpretation: Econ. Geol., v.58, p.167-211.
- (1972) Composition of fluid inclusions: U. S. Geol. Survey Prof. Paper 440-JJ, 164p.

- (1979) Fluid inclusions as samples of ore fluids, in Barnes, H.L. ed., *Geochemistry of Hydrothermal Ore Deposits*: 2nd edition, New York, Wiley and Sons, p.684-737.
- (1979) Fluid inclusions studies on the porphyry-type ore deposits at Bingham, Utah, Butte, Montana, and Climax, Colorado: *Econ. Geol.*, v.66, p.98-120.
- Roedder, E., Heyl, A.V., and Creel J.P. (1968) Environment of ore deposition at the Mex-Tex deposits, Hansonburg district, New Mexico, from studies of fluid inclusions: *Econ. Geol.*, v.63, p.336-348.
- Roedder, E., Ingram, B., and Hall, W.E. (1963) Studies of fluid inclusions III: Extraction and quantitative analysis of inclusions in the milligram range: *Econ. Geol.*, v.58, p.353-374.
- Rye, R.O. and Haffty, J. (1969) Chemical composition of the hydrothermal fluids responsible for the lead-zinc deposits at Providencia, Zacatecas, Mexico: *Econ. Geol.* v. 64, p629-643.
- Sweeting, M.^MJ. (1973) *Karst Landforms*: New York, Columbia University Press, 362p.
- Thornbury, W.D. (1969) *Principles of Geomorphology*, 2nd edition: New York, Wiley and Sons, 594pp.
- Weimer, R.J. (1978) Influence of transcontinental arch on Cretaceous sedimentation: A preliminary report, in *Rocky Mountain Association of Geologists 1978 Symposium*, p211-222.
- (1979) Influence of basement tectonics depositional systems and seismic stratigraphy abs. : AAPG-SEPM Annual Convention, April 1-4, Houston, Texas, p186.

APPENDIXES

(A-1)

Appendix A

Tables of values used in Thermodynamic Calculations

TABLE I. CALCULATED AVERAGES: CONCENTRATION (ppt), MOLALITY AND MILLIEQUIVALENTS

	Ca	Mg	K	Na	Zn	Cu	Pb	Fe	Cl	F
GALENA										
ppt	8.44	.096	5.81	51.48	.58	-	*	.107	95.61	.925
Molality	.25	.0047	.18	2.67	.01	-	*	.002	3.22	.058
Milliequivalents	.50	.0094	.18	2.67	.021	-	*	.004	3.22	.058
FLUORITE										
ppt	*	.60	2.04	45.1	.06	.290	3.14	.602	23.95	*
Molality	*	.027	.058	2.18	.001	.005	.017	.012	.75	*
Milliequivalents	*	.054	.058	2.18	.002	.010	.034	.024	.75	*
QUARTZ										
ppt	6.15	.101	1.60	42.80	7.31	1.86	6.50	1.09	46.10	.868
Molality	.17	.0046	.046	2.07	.13	.033	.035	.022	1.46	.051
Milliequivalents	.34	.0092	.046	2.07	.26	.066	.070	.044	1.46	.051

* - High Concentration due to Mineral Solubility

- - - None Detected

TABLE II. SUMMARY TABLE FOR VALUES OF EQUILIBRIUM
CONSTANTS USED IN THERMODYNAMIC CALCULATIONS

<u>EQUILIBRIUM EQUATIONS</u>	<u>Log K</u>	
	<u>150°C</u>	<u>200°C</u>
$\text{CO}_2(\text{g}) + \text{H}_2\text{O} = \text{H}_2\text{CO}_3(\text{ap})$	-2.07	-2.06
$\text{CaCO}_3 + 2\text{H}^+ = \text{Ca}^{++} + \text{H}_2\text{O} + \text{CO}_2(\text{g})$	9.04	8.95
$2\text{H}^+ + \text{S}^= + \frac{1}{2}\text{O}_2 = \frac{1}{2}\text{S}_2 + \text{H}_2\text{O}$	37.33	34.05
$2\text{H}_2\text{O} + \text{S}_2 = \text{O}_2 + 2\text{H}_2\text{S}(\text{ag})$	-39.99	-35.05
$\text{Pb}^{++} + 4\text{Cl}^- = \text{PbCl}_4^=$	2.57	3.2
$\text{PbS} + 2\text{H}^+ + 4\text{Cl}^- = \text{PbCl}_4 + \text{H}_2\text{S}(\text{ag})$	-2.03	.64
$\text{H}_2\text{CO}_3 = \text{H}_2\text{O} + \text{C} + \text{O}_2$	-46.67 ^A	-41.49 ^A
$\text{CO}_2 = \text{C} + \text{O}_2$	-48.74	-43.55
$3\text{FeS}_2 + 2\text{O}_2 = \text{Fe}_3\text{O}_4 + 3\text{S}_2$	+40.95	+38.11
$2\text{FeS}_2 + 3/2\text{O}_2 = \text{Fe}_2\text{O}_3 + 2\text{S}_2$	34.66	31.72
$\text{FeS}_2 = \text{Fe}^{++} + \text{S}^= + \frac{1}{2}\text{S}(\text{g})$	-26.60	-24.19
$\text{FeS} = \text{Fe}^{++} + \text{S}^=$	-16.33	-15.71
$\text{FeCO}_3 = \text{Fe}^{++} + \text{CO}_3^=$	-12.86	-14.05
$\text{PbS} = \text{Pb}^{++} + \text{S}^=$	-21.93	-20.36
$\text{PbSO}_4 = \text{Pb}^{++} + \text{SO}_4^=$	-8.26	-8.88
$\text{PbCO}_3 = \text{Pb}^{++} + \text{CO}_3^=$	-13.54	-14.30
$\text{ZnS} = \text{Zn}^{++} + \text{S}^=$	-21.01	-19.81
$\text{ZnCO}_3 = \text{Zn}^{++} + \text{CO}_3^=$	-11.77	-12.90
$\text{H}^+ + \text{CO}_3^= = \text{HCO}_3^-$	10.29	10.68
$\text{HCO}_3^- + \text{H}^+ = \text{H}_2\text{CO}_3$	6.73	7.08
$\text{SO}_4^= = 2\text{O}_2 + \text{S}^=$	-96.68	-83.74
$\text{CaSO}_4 = \text{Ca}^{++} + \text{SO}_4^=$	-6.35	-7.18
$\text{BaSO}_4 = \text{Ba}^{++} + \text{SO}_4^=$	-9.34	-9.76
$\text{H}_2\text{S} + 2\text{O}_2 = \text{H}^+ + \text{HSO}_4^-$	83.05	71.62
$\text{H}_2\text{S} + 2\text{O}_2 = 2\text{H}^+ + \text{SO}_4^=$	79.31	67.13
$\text{HS}^- + 2\text{O}_2 = \text{H}^+ + \text{SO}_4^=$	86.03	74.09
$\text{H}_2\text{S} = \text{H}^+ + \text{HS}^-$	-6.72	-6.96
$\text{HS}^- = \text{H}^+ + \text{S}^=$	-10.62	-9.57

All equations from Helgeson (1969) with exception of (A) Ohmoto (1972)

TABLE III. SUMMARY TABLE FOR VALUES OF: MOLALITY, ACTIVITY COEFFICIENTS AND ACTIVITIES USED IN THERMODYNAMIC CALCULATIONS.

	Ca		Fe		Pb		Zn	
	150°C	200°C	150°C	200°C	150°C	200°C	150°C	200°C
Log m	-.77	-.60	-1.66	-2.70	-1.46	*	-.89	-2.0
Log γ^A	-.88 ^B	-1.02 ^B	-.90 ^C	-1.0 ^C	-3.0 ^C	-3.6 ^C	-3.8 ^C	-5.0 ^C
Log Activity	-1.65	-1.62	-2.56	-3.70	-4.46		-4.69	-7.0

	Cl		F		SO ₄		H ₂ S, H ₂ CO ₃	
	150°C	200°C	150°C	200°C	150°C	200°C	150°C	200°C
Log m	.164	.508	-1.29	-1.24	-3.56	-4.09	-.59	-.64
Log γ^A	-.298	-.356	-.26	-.30	-1.14 ^D	-1.47 ^B	.16 ^D	.24 ^D
Log Activity	-.134	.152	.14	-.87	-4.7 ^E	-5.56 ^E	-.43	-.40

A - Stoichiometric Individual Ion Activity Coefficient

B - Calculated from Debye-Huckel Equation (Helgeson, 1967)

C - Helgeson (1969)

D - Interpolation of Data From: Ohmoto (1972)

E - Calculated From Anhydrite Equilibrium and Analysed Ca Values

TABLE IV. COMPOSITION OF FLUID INCLUSIONS FROM CAVE-IN-ROCK FLUORITE DISTRICT, ILLINOIS

Mineral	Weight Extracted H ₂ O (mg)	Dilution Factor	Composition						Atomic ratios			
			Ca (ppm)	Mg (ppm)	K (ppm)	Na (ppm)	Cl (ppm)	SO ₄ (ppm)	K/Na	Ca/Na	Cl/Na	
Yellow fluorite	23.4	**	*	2,100	2,400	45,200	84,000	3,400	0.031	0.077	1.21	
Yellow fluorite	12.9	**	*	1,300	2,800	49,000	94,000	2,200	.035	.096	1.24	
Early white fluorite	15.9	**	*	900	1,400	23,000	47,300	1,200	.036	.12	1.34	
Blue fluorite	6.2	**	*	6,600	2,700	40,000	94,000	5,000	.040	.17	1.53	
Blue fluorite	1.6	**	*	5,700	3,000	47,000	98,000	3,900	.037	.099	1.35	
Early purple fluorite	2.9	**	*	6,100	3,200	41,000	78,000	5,900	.046	.061	1.22	
Quartz	8.3	**		8,400	2,900	4,300	17,300	47,000	12,900	.141	.28	1.75
Sphalerite	7.0	**		17,000	2,200	2,500	27,000	59,000	*	.055	.36	1.42
Galena	5.5	**		20,600	4,000	3,100	55,400	115,000	*	.033	.21	1.34
Late purple fluorite	4.3	**	*	1,000	2,000	43,300	87,000	900	.027	.085	1.30	
Late purple fluorite	1.9	**	*	11,000	5,100	60,200	134,000	6,400	.050	.078	1.44	
Late purple fluorite	5.0	**	*	6,000	3,800	43,200	93,000	1,300	.052	.087	1.40	
Late purple fluorite	3.0	**	*	4,000	3,800	50,500	100,000	1,900	.044	.047	1.28	
Barite	4.3	**		11,000	2,000	4,100	4,500	4,000	*.54	1.40	.57	
Witherite	1.0	**		7,500	1,400	6,100	7,500	14,300	high ¹	.48	.57	1.24
ANALYSIS FROM OTHER MISSISSIPPI VALLEY-TYPE DEPOSITS												
Sample No.												
<u>Cave-In-Rock</u>												
ER59-10M ¹	6.9	15,300	*	7,040	4,440	50,490	108,630	1,530	.05	<.91	1.40	
ER59-10P	NR ^(6.9)	* (4,650) ²	*	7,530	3,860	76,730	152,520	<470	.03	<.45	1.29	
ER59-10a	2.6	8,080	*	4,690	4,360	58,980	116,350	2,260	.04	<.44	1.28	
<u>Rosiclare</u>												
ER59-15	0.44	16,360	*	<3,270	6,380	71,980	130,880	65,440	.05	<.14	1.18	
ER59-15 ₂	NR ^(.44)	(100,230) ²	*	21,050	28,060	270,621	601,380	65,150	.06	<1.7	1.44	
<u>Cave-In-Rock</u>												
ER59-10M ¹	(10)	10,580 ²	*	4,870	3,070	34,910	75,120	1,060				
ER59-10P	(10)	3,210 ²	*	5,200	2,660	52,970	105,290	<320				
ER59-10a	(4)	5,250 ²	*	3,045	2,840	38,330	75,600	1,470				
<u>Rosiclare</u>												
ER59-15	(1)	7,200 ²	*	<1,440	2,810	31,680	57,600	28,800				
ER59-15 ₂	(1)	44,100 ²	*	9,260	12,350	119,070	264,600	28,670				

¹ SO₄ was not analyzed, but it probably is high to account for the deficiency of analyzed cations.

Analysis from Cave-In-Rock from: Hall and Friedman (1963)

* - High Concentrations due to Mineral Solubility

** - Not Reported

NR - Not Recovered

() - Weight H₂O (mg) by visual estimate

² Calculated on visual estimate of H₂O

Analysis from: Roedder, Ingram, Hall (1963)

TABLE V. COMPOSITION OF FLUID INCLUSIONS FROM UPPER MISSISSIPPI VALLEY ZINC-LEAD DISTRICT, WISCONSIN, ILLINOIS, AND IOWA

Mineral	Amount of inclusion water recovered (milligram)	Composition						Atomic Ratios				
		Na (ppm)	K (ppm)	Ca (ppm)	Mg (ppm)	Cl (ppm)	SO ₄ (ppm)	K/Na	Ca/Na	Mg/Na	Cl/Na	SO ₄ /Na
Sphalerite Amelia mine	18.0	53,400	2,500	20,400	2,200	120,000	*	0.028	0.37	0.37	1.46	*
Galena, Amelia mine	5.5	39,000	3,200	18,500	3,400	83,000	*	.048	.46	.082	1.37	*
Pink calcite stage 1, Piquette mine	7.7	9,100	800	*	1,200	17,400	1,800	.048	*	.12	1.25	.047
Calcite Stage 2 Bausche mine	8.7	19,000	800	*	1,700	31,800	7,500	.022	*	.084	1.08	.093
Calcite Stage 3 Amelia	11.9	16,800	600	*	1,200	21,400	3,600	.020	*	.069	.82	.051

Analysis from: Hall & Friedman (1963)

* - High concentrations due to mineral solubility

TABLE VI. COMPOSITION OF FORMATION WATERS

	Ca	Mg	K	Na	Cl (+Br)	SO ₄
BEULAH SIMON						
BS2 01	2,190	250	462	27,400	52,300	420
BS2 03	2,850	250	472	29,700	53,300	412
BS2 05	2,870	250	444	30,300	53,800	464
BS2 09	2,880	250	486	23,200	53,600	284
BS2 10	2,900	260	487	28,800	55,200	360
BS2 11	3,000	260	478	29,500	56,100	344
PLEASANT BAYOU						
PB2 09	8,680	640	534	37,400	73,900	<5
PB2 11	9,090	670	587	35,500	83,000	<5
PB2 19	8,450	640	540	36,000	80,300	
PB2 21	8,650	640	548	37,000	78,400	
PB2 22	8,640	630	560	37,200	79,800	
PB2 27	9,210	670	573	39,800	84,200	
PB2 28	3,390	1,130	202	44,600	99,500	
FAIRFAX-FOSTER-SUTTER						
FFS 01	5,500	640	820	43,700	91,800	<5

Analysis from: Randolph et al. (1980)

Appendix B

Fluid Inclusion Study

Microthermometry

Procedure

The procedure entailed freezing to -100 C and slowly raising the temperature through solid and liquid phases to the homogenization temperature, usually around 160 C, and was performed upon .3 to .7mm doubly polished thick sections, with the aid of a LINKAM heating and freezing stage. For more detailed description of the above procedures and equipment, the reader is referred to Appendix C. Daily verification of known melting points (-60 to 200 C) for both organic and inorganic compounds determined the calibration curve for each day's use, and in general reflected an accuracy for measurements within ± 0.5 C.

Types of Inclusions

Inclusions of Primary, pseudosecondary, and secondary types were observed. Criterion used for

distinction were adopted after Roedder et al., (1968), Freas (1961) and others. Primary types were quite abundant in all minerals examined and proved to possess homogenization temperatures usually in accordance with the pseudosecondary types from the same immediate area (Roedder et al., 1968 p 344 fig 13) but significantly greater than those from both secondary types occupying rather obvious sealed fractures, and pseudosecondaries from later growth stages.

Sphalerite

In sphalerites, inclusions were very abundant, though locally areas were both correspondingly void of inclusions, and increasingly yellow in color. These were correlative to areas of certain growth bands, but their spotty discontinuous nature is a bit of a dilemma.

Primary types within the sphalerites showed some of the more intense necking down observed, and were in much greater ratio to pseudosecondary or secondary types than other mineral species. Though most primaries showed evidence of necking down, and thus were not useful in the heating-freezing procedures,

many were suitable and provided good, reproducible data. Venting was not observed within the sphalerites examined.

Solid phases and trashy material occluded much of the sphalerite either as isolated grains or in planes parallel to growth faces. Solid phases are predominantly quartz, though barite is also quite prevalent.

Fluorites

In fluorites, the primary types were commonly rather large, very angular, cubic to box-like isolated inclusions. Some of the more regular inclusions permitted actual measurements of their dimensions via micrometer eyepiece, and focusing ring.

In addition to the primary types are the abundant planes of pseudosecondary and some secondary type inclusions. These are often found proximal to and locally parallel to growth faces, whose identity is revealed by the abundance of solid phase included crystals, which invariably point upwards in the direction of growth of the host (see text photographs).

Quite noticeable in these micrographs accompanying the solid crystals are "spines", which in reflected light reveal a brass yellow color and pyritic to

chalcopyritic appearance. There is no regular form for these included sulfides as is evidence in the variety of shapes and sizes observed. Robert H. Weber, Senior Geologist and the Mineralogist for New Mexico Bureau of Mines and Mineral Resources was consulted for identification based upon crystal form. Weber could not determine definite identification, due to the high variability of forms, as stated above. He did confirm, however, my initial identification as some sort of sulfide; predominantly iron with perhaps minor copper.

Another attempt at identification yielded qualitative but not quantitative data on the sulfide's chemistry. The scanning electron microscope (SEM) was employed here (see SEM section in text), as it was felt by the author that the spines could possibly be exposed by fracture, located and examined at great magnification and identified by use of an X-ray analyzer beam, incorporated within the microscope (Metzger and others, 1975; Sawkins, 1979).

In general the data obtained reflect, as expected, predominance of iron and sulfur, with local high responses for copper, followed by much lower responses for lead and locally zinc.

Crystallographic determination by X-ray diffraction was not attempted due to the highly varietal form of the sulfides. It was felt that if these were "trashy" sulfides, no conclusive identity

could be ascertained by this method, but rather that each individual crystal would possess differing crystallographic parameters.

As visible in the photomicrographs, these spines are oriented with their long dimension parallel to the direction of growth. Most seem to have started as a minute crystal, originally deposited upon the fluorite growth face, which continued to grow, as did the fluorite. Physically it appears that the fluorite confined the sulfide, enabling it to grow only in the long dimension, showing slight local thickening as it progressed. Chemically it appears as though the sulfide crystal, once deposited upon the fluorite surface, continued to "pull" from solution the necessary constituents for growth (iron, sulfur, copper plus or minus lead and zinc) The zones of increased thickness could indicate periods of slower growth in the fluorite; periods of increased iron and sulfur concentrations; or perhaps a combination of both. These models would also perhaps explain the characteristic stepped or angular nature of the zone of increasing thickness. This is supported by the occurrence, during freezing, of annular rings of H₂S (?) surrounding the vapor phase, as described by Roedder (1971, p101-103). This was observed only within the inclusions from this sample with its included sulfides.

During the homogenization of fluorite samples, it was noted that some chips, once heated to homogenization temperatures, exhibited increased temperatures upon successive runs. In conjunction with this, observations of the movements of some vapor bubbles preferentially toward a "suture" area indicated that at the high temperatures required for homogenization, internal pressures built up significantly, forcing fluid out along the previously sealed sutures. Because of this, the fluorite samples were first examined and photographed, then broken into very small (0.5 cm. sq.) chips for use on the heating-freezing stage, and the homogenization data taken as valid from only the initial heating stage. When performed in this manner, all chips from a given sample yielded data in agreement with adjoining chips. Quartz did not exhibit this phenomena, yielding identical temperatures no matter how often rerun.

Quartz

In quartz samples, primary types most commonly exhibited negative crystal form, some with crystallographic planes visible within. Some also contained the small highly birefringent "speck" discussed in the preceding fluorite section. Pseudosecondaries were not as prevalent here as in

(B-7)

other species, though the inclusion of solid material was nearly so.

Appendix C

Procedures and Equipment

Heating-Freezing Stage

The TH600 heating-freezing stage used in this study proved to be very versatile, as it enables the selection of heating rates from 0.1 to 90.0 degrees per minute. The minimum temperature attainable with this apparatus (using liquid nitrogen) was -178 C and the maximum attainable was 600 C. Features included a "limit-set" which set a maximum temperature not to be exceeded by the heating element, and a "hold" button which allowed for the instantaneous stopping of the heating "ramp". With careful adjustment of the cooling gas flow, a cooling "ramp" could be established which utilized the heating element as the control. In this manner both heating and cooling rates could be controlled, enabling very precise control over temperature induced phenomena.

Small chips of samples were mounted on the heating element interior to the walls and the contained water jacket. Light was transmitted via a sapphire window in the center of the stage. Temperature was monitored by a platinum resistance element inserted into the heating

element, and displayed as degrees centigrade on the control unit. Samples were frozen first to determine salinity attributable phenomena, and then homogenized. This order was preferred as some samples would exhibit venting phenomena during homogenization heating, and measurements made after this were subject to scrutiny.

Preparation of Thick Sections

Selection

Thick sections for use on the heating-freezing stage were prepared for each sample to be examined. This entailed hand selection of no less than two suitable samples from each bulk field sample. These samples were to be representative of the bulk sample and taken in duplicate to enable double-checking of any heating or freezing data. These hand selected specimens were carefully examined and diagramed in order that interior location of inclusions could be kept relative to growth stages within the crystal. This enabled the potential for observations regarding variations in temperature and/or salinity to be located on the diagram as one examined the various crystals.

Polishing Procedure

Samples were cut creating a flat surface parallel to the desired plane of inspection. This surface was then worked smooth starting with a -200 grit silicon carbide powder on a aluminum-faced polishing wheel, and progressively diminishing grit size until the sample had been hand-rubbed on a glass plate using -600 grit silicon carbide powder. The sample was then placed in the ultrasonic cleaner to remove any remaining grit particles. Brass polishing wheels covered with fine "metcloth" muslin were used for finishing polishes with 1.0 alpha and 0.05 gamma (microns) alumina (AL2O3) successively.

Samples with a suitable polish on the one side were mounted to glass slides using Aremco Crystalbond 509. This was found superior to all other methods due to the strength of the adhesive, its clear nature and its solubility in acetone. Mounting was performed on a hot-plate, and samples were ready for further polishing well within ten-minutes. Once firmly mounted, the opposite side of each sample was prepared as described above, except that the samples are held in glass slide mounts while being worked down.

Previous to the final polishing stages, samples were ground using a facing wheel to a thickness averaging less than 0.5mm, as this enabled a good

thickness for the possibility of locating any inclusions, and would leave a reasonably competent sample once removed from the mounting. This is a suitable thickness only for those minerals which are light colored and transparent. Sphalerite proved to be locally too dark for this thickness, but overall provided no problems. Galena, due to its opaque nature was impossible to examine in the transmitted light microscope, and thus was not prepared in the above manner.

Examination of "Thick" Sections

Once completely polished on both sides, samples were then inspected through the microscope before removal from mounting. The clear mounting medium was useful here because if a sample was noted as having an insufficient polish, the specimen was still in a well supported form for further work.

Complete diagrams were made of each thick section in order that observations made while examining the microscopic properties of the sample could be located and noted for later compilation of the characteristics of each sample or group of samples. Areas which were very inclusion rich or possessed any other notable characteristics were photographed or located on the drawing. Samples were then broken (cleaved) so that

(C-5)

individual chips from the same sample could be run on the heating-freezing stage without over-heating the entire sample. These chips were also located on the diagram so their relation to the crystal growth zones could be kept straight, and any temperature zonations within one crystal would be noted.

Cleaning Procedures

Samples

Samples were hand selected to eliminate waste and maintain sample homogeneity, washed in distilled water and put into the ultrasonic cleaner to open major cracks and remove any excess debris. Samples averaged one centimeter cubed as very small chips and fines were eliminated due to their low inclusion density to surface area ratio, which makes them undesirable.

Samples were then simmered in reagent grade HNO₃ (100%) for 24-hours, dependent upon mineral solubilities, and then rinsed with two ten-minute rinses in 100% HF, stored in precleaned Teflon beakers and covered with distilled doubly-deionized water, until entered into electrolytic cells. Should any contaminants enter the beaker, they would hopefully go into and remain in solution.

Electrolytic cells are a major part of the cleaning procedure, requiring 3-5 days dependent upon the mineral being cleaned. A potential of 30 milliamps is placed across two platinum electrodes, each at opposite ends of a U-shaped quartz tube. These tubes are filled with distilled doubly-deionized water, enough to cover the sample and to reach both electrodes. Water is changed frequently, starting at

4-hour intervals and working upwards to 24 hours dependent upon the milliampere reading for each individual cell. The process is considered complete when the milliamp reading remains less than or equal to 5, for at least a 24-hour period.

The completed samples were then placed into their precleaned stainless-steel extraction tubes for storage until use. If usage is not immediate, the tubes containing samples must be dried, as any water remaining in the tubes could leach contaminants from the walls of the tubes. My samples were extracted immediately following entry into the tubes and the vacuum in the extraction line was utilized to create dryness. This was done in order to minimize contamination potential from storing samples over a period of time.

Extraction Tubes

The extraction tubes were constructed from type 304 stainless-steel thin-wall, three-quarter inch diameter tubing. This was cut into approximately 13 inch lengths, crimped at one end with a 50-Ton hydraulic press, and arc-welded shut. The other, open end was burnished and filed to prevent any rough edges and insure a good seal on the vacuum line. This type of tubing was preferred over others due to its

durability, which allowed for a complete crush and subsequent rerounding without loss of internally held vacuum. In addition, it was hoped that any contamination resultant from the walls of the tube would not effect those metal values most interesting to this study. For this reason copper tubing was not suitable.

Once formed into and prepared for sample extraction tubes, they were completely immersed in 100% HNO₃ for 18-24 hours, followed by 15-20 good rinses with distilled water. Each was then covered and set aside for later use. Tubes were never touched until samples were entered and isolated from contamination. Prior to sample entry, each tube was subjected to 15-20 rinses with distilled doubly-deionized water, and then connected to the vacuum line immediately following sample entry.

Glassware

All glassware, including Teflon labware, were subject to the same intense cleaning procedure used on the extraction tubes and samples. This included 24 hour simmering in reagent grade 100% HNO₃, followed by a 24 hour boiling in distilled water, and storage in evacuated "zip-lock" bags. Glassware was never touched until ready for use, and polyethylene gloves were used

(C-9)

wherever possible.

Extraction Procedure

Equipment

Crushing Device

The device used for crushing the stainless steel extraction tubes was constructed out of a Sears 5-Ton hydraulic jack and two parallel mounted flat steel bars. One bar remained the fixed "jaw" and the other was mounted to the top of the jack. The tubes were placed between the jaws and crushed in small "bites" working down from the top level of sample in the tube. Reversing the above process re-rounded the tubes enabling for later sample removal for the leaching process.

Vacuum Line

The vacuum line as constructed was entirely Pyrex tubing except for the sample junction site and capillary trap at the extreme right end of the line.

Pressure was monitored using a McLoed "swivel-gauge" manometer which contained both linear and non-linear scales. The non-linear scale provided for pressure readings less than 1.0mm Hg, and thus was

the preferred scale for the extraction work.

Samples were entered onto the line by means of a brass Cajon fitting for 3/4 inch tubing. The fitting contained a soft inert "O" ring which was compressed around the outside of the tubing to insure a vacuum tight seal. Small amounts of vacuum grease were applied to the outside of the tubing to aid the "O" ring in it's seal.

At the extreme end of the line a capillary trap was added for the entrapment of sample vapors by immersing the capillary in liquid nitrogen and freezing them there. The capillary was then sealed shut with the light touch of a torch at a point well above the trapped vapor, and allowing the vacuum within the line to seal it shut. All capillaries were carefully weighed before entering onto the line, which enabled the calculation of the extracted waters weight by subtracting that initial weight from the final capillary weight.

Vacuum was attained in the extraction line using a simple Welch rotary oil pump. Though just a roughing pump, it proved more than sufficient for desired vacuum.

Methods

Extraction Technique

Once the extraction line had been evacuated for a sufficient period to allow for de-gassing, it was required to maintain a pressure of 2-5 microns for a 4-8 hour period, before any extractions were attempted. This was to insure against the loss of vacuum once a sample was entered onto the line. Sample extraction tubes were then entered on the line and evacuated to a pressure of 2 microns, and held there a period of 30-60 minutes to allow for slight sample de-gassing, and the popping of cracks and some major secondary inclusion planes.

The sample was then sealed off from the line and removed at a ball-in-socket junction while maintaining the vacuum in the extraction tube. The sample was then carefully crushed and the tube returned to a near round shape, and joined back with the line. Caution must be exercised so that the vacuum inside the tube is not lost.

Pressure readings were taken prior to opening the extraction tube into the vacuum line to insure that a full vacuum was being maintained. A liquid nitrogen bath was put on the trap and the sample extraction tube was allowed to vent into the vacated line. After a

period of 5-7 hours, the valve was closed and the pressure noted. An acetone-dry ice bath replaced the liquid nitrogen bath, and the pressure was allowed to equilibrate (15-30 minutes). These two pressures made possible calculations regarding relative amounts of CO₂ gas, and also would have shown the presence of any non-condensable gasses during the initial pressure reading while using the liquid nitrogen bath.

A liquid nitrogen bath was then put on the capillary trap, as described above, before the removal of the dry ice bath, to create a low pressure region, and "attract" all the vapor particles in that direction. The liquid nitrogen bath was started at the very bottom of the capillary tube and slowly moved upward. This was to prevent blockage of the capillary by ice crystals, and to more efficiently trap the vapor. Once the capillary was filled it was sealed in the manner described above, and the water weighed.

Once the sample extraction tube has been isolated from the extraction line by means of a valve, it may be removed and isolated from contamination by sealing the top with Para-seal, and then covering with tin-foil, and sealing with masking tape and storing until ready for use. The tubes make exceptionally good storing places as they are isolated from any water and contaminants while inside the tube. Also by this manner all samples, or group of samples could then be

leached at one time.

Leaching Procedure

Samples that have been crushed and been evacuated on the vacuum line were then poured out of the stainless steel tube into a precleaned teflon beaker which contained 20 ml. distilled doubly-deionized water and covered with para-film to guard against contamination. The tube was discarded as these proved to be intense sources of contamination if they were rinsed with water and added to the leach solution. The crushed material was allowed to soak in the teflon beaker for 10-20 minutes, and the supernatant liquid is decanted into a filter-vac set up for retrieval of the filtrate, or leach solution. This decantation procedure was repeated 4-5 times.

This leach process is the most likely spot for contaminants to enter the solution, and hence strict attention must be paid to cleanliness. Polyethylene gloves should be worn at all times in addition to a relatively clean lab coat.

Leach blanks should be run through the leach process periodically along with a group of samples, in order that any contamination could be traced back to its source.

Once sufficient decantate exists, it should be poured off into linear polyethylene bottles, which have been precleaned and then rinsed with 2-4 rinses of distilled doubly-deionized water, and labelled with the sample name.

It is preferable to keep minimized the total volume of leach solution as increased volume is equivalent to increased dilution factor, which makes minor elements difficult to detect. However, while keeping the leach solution to a minimum volume one must be certain to use sufficient water and time to be certain that all water soluble species are extracted from the crushed material.

A conductivity meter should prove useful here in monitoring the relative amount of dissolved ions. In this study extensive preliminary runs were performed, using prepared "sample" solutions which were sealed in pre-cleaned capillary tubes and placed in extraction tubes along with pre-cleaned pure quartz rod (for bulk), and crushed, extracted and analysed identically to the samples. The solution entered into the capillary tubes was prepared in such a way as to approximate those concentrations reported from other fluid inclusion analysis. In this manner experimentation led to the final procedures which were most suitable for this type of research.

This thesis is accepted on behalf of the faculty of the

Institute by the following committee:

David d. Norman
Adviser

K. C. Condie

Carl J. Voss

F. J. Kullberg

21 Nov. 1980
Date